Title: Prenatal Arsenic Exposure and Gene Expression in Fetal Liver, Heart, Lung, and Placenta

Author names & affiliations (with ORCIDs):

K. A. Rychlik[1,2] (ORCID: 0000-0001-5766-0913)

C. Kashiwagi[1] (ORCID: 0000-0002-6524-3236)

J. Liao[1]

A. Mathur[1]

E. J. Illingworth[1] (ORCID: 0000-0003-1224-2990)

S. S. Sanchez[1] (ORCID: 0000-0002-3649-778X)

A. Kleensang[1] (ORCID: 0000-0002-4564-7399)

A. Maertens[1] (ORCID: 0000-0002-2077-2011)

F. C. M. Sillé[1] (corresponding author; address: Johns Hopkins Bloomberg School of Public Health, 615 N. Wolfe st. RM E7628, Baltimore, MD 21205; email: fsille1@jhu.edu) (ORCID: 0000-0003-4305-2049)

1 Department of Environmental Health and Engineering, Bloomberg School of Public Health, Johns Hopkins University, Baltimore, MD, USA

2 Public Health Program, School of Health Professions, Mayborn College of Health Sciences, University of Mary Hardin-Baylor, Belton, TX, USA

Keywords: arsenic, prenatal, mRNA, microarray, immune

Running Head: Prenatal Arsenic: Gene Expression in Multiple Fetal Tissues

Abstract

Prenatal arsenic exposure has been linked to a myriad of negative health effects. There is relatively little insight into the mechanisms and signaling alterations across different fetal organs that drive long-term immune-related issues following prenatal arsenic exposure. Therefore, the effects of this exposure window on gene expression in the liver, placenta, heart, and lung of gestation day (GD) 18 C57BL/6 mouse fetuses were investigated. From two weeks prior to mating until tissue collection at GD18, mice were exposed to 0 or 100 ppb sodium (meta) arsenite in drinking water. Genes of interest were analyzed by RT-qPCR, complemented with untargeted Agilent 44K microarray analysis. Data cleanup and analysis was performed in RStudio. Differentially expressed mRNAs were queried in the String Database and using Cytoscape to create interaction networks and identify significantly enriched biological pathways. A total of 251, 165, 158, and 41 genes were significantly altered in the liver, placenta, heart, and lung, respectively, when treated samples were compared to controls. Many altered pathways were immune-related, supporting prior research. Most notably, gene expression of Gbp3, a key player in the cellular response to interferon gamma, was found to be reduced in placentas of female fetuses exposed to arsenic compared to controls (p=0.0762).

Impact: This is the first study comparing alterations in gene expression across multiple organs following prenatal exposure to environmentally relevant levels of arsenic. These findings, elucidating the multi-organ impact of prenatal arsenic exposure on predominantly immune-related pathways, further our mechanistic understanding of the long-term health effects observed in early-life arsenic-exposed populations.

Introduction (<=750 words)

Despite strong population-level data supporting the association between prenatal inorganic arsenic exposure and cancer of the liver and lung, heart disease, and immune dysfunction (Smith et al. 2012; Naujokas et al. 2013; Khan et al. 2020), the mechanisms driving these long-term effects are still unclear. Arsenic is the most common chemical drinking water contaminant worldwide and puts roughly 230 million people at risk (Shaji et al. 2021), including the most vulnerable populations of pregnant women and children. Within the U.S. alone, an estimated 2.1 million people are drinking water contaminated with levels of arsenic higher than the recommended limit of 10 ppb (Ayotte et al. 2017).

In an effort to isolate the mechanisms driving effects, some work has turned to investigating the placenta. Identified as a route of early exposure to arsenic (García Salcedo et al. 2022), the placenta is a mediator of *in utero* exposure and, in the case of heavy metals, could provide an indication of altered signaling in the neonate due to maternal exposure (Myllynen et al. 2005). Early evidence, albeit at rather high doses (20 ppm), indicate disruption of placental vasculogenesis (He et al. 2007) which could result in placental insufficiency, a condition which, like arsenic, has been associated with fetal (or intrauterine) growth restriction (IUGR) (Neerhof and Thaete 2008; Xu et al. 2022).

In a U.S. cohort study of low-to-moderate levels of arsenic exposure during pregnancy, alterations in gene expression and the epigenetic profile of placental tissue were discovered with differences noted between male and female fetal sex (Winterbottom, Ban, et al. 2019; Winterbottom, Moroishi, et al. 2019). Although not identified in that cohort, one pathway that has been presented as a possible mediator for IUGR after prenatal arsenic exposure is the glucocorticoid receptor signaling pathway (Caldwell et al. 2015). Not only is this pathway essential for many endocrine functions but it is also plays a key role in metabolism and immune function (Kadmiel and Cidlowski 2013). Dose-dependent effects on glucocorticoid signaling has also been identified in JEG-3 cells, an *in vitro* model of trophoblasts

(Meakin et al. 2019). Specifically, Meakin et al. (2019) identified DNA methylation as a driver of effects within that pathway. Epigenetic alterations and gene expression changes have also been identified in newborn mouse liver tissue following *in utero* exposure to 85 ppm arsenic (Xie et al. 2007).

In human cohorts, gene expression and cytokine levels have been affected in cord blood based on maternal arsenic exposure levels (Fry et al. 2007; Rager et al. 2014). In an integrative study of data from twelve prior cohort studies in humans looking at CpG methylation, gene expression, or protein expression in the placenta or cord blood, Laine & Fry (2016) determined that many of the commonly altered genes were related to immune and inflammatory pathways.

The question of whether gene expression alterations in the placenta at birth correspond to alterations in other organs and whether those alterations are mechanistic drivers for long-term disease, however, has yet to be answered. Therefore, this research set out to determine what gene expression alterations, if any, occurred following preconception and prenatal exposure to inorganic arsenic in drinking water among placenta, liver, heart, and lung tissues in the C57Bl/6J mouse model. Initially, genes of interest were selected to quantify using RT-PCR in each organ based on prior research and networks of interest, particularly in the intersection between the immune system and glucocorticoid signaling. Secondarily, a microarray was performed on a subset of samples to investigate larger network alterations and trends.

Materials and Methods

Animal Care and Mouse Exposure Model

Despite some interspecies differences, C57BL/6 mouse models have been proven representative for assessing arsenic immunotoxicity (Ramsey et al., 2013a; Ramsey et al., 2013b; Kozul et al., 2009). Breeder male and female C57Bl/6J mice (8 weeks of age) were obtained from Jackson Laboratories (Bar

Harbor, Maine). Mice were given a week to acclimate prior to experiments. Male mice were housed individually. Female mice were housed individually at the onset of arsenic exposure in order to accurately monitor food and water intake. Enrichment was added to cages including a mouse igloo and additional sterile paper bedding material. Cages were housed in a temperature and humidity-controlled facility with 14:10 light:dark cycle and provided *ad libitum* access to food and water. Low arsenic chow diet was obtained from Research Diets Inc. (AIN-93M). ***Exposure model:*** Mice were evenly distributed (by weight) into two groups two weeks prior to mating: Control with access to plain water (0 ppb iAs) and Exposure with access to exposure water (spiked with 100 ppb iAs - a relevant dose in many areas of the world (Ayotte et al. 2017; García Salcedo et al. 2022; Naujokas et al. 2013) - in the form of sodium(meta)arsenite (CAS# 7784-46-5) obtained from Millipore Sigma [St. Louis, MO]). All water was provided to the mice in glass containers to avoid risk of phytoestrogen interference in the study. Crystal Springs brand water (Lakeland, FL), with reported non-detectable levels of arsenic, was refreshed every 3-4 days to avoid arsenic oxidation. No significant differences in water or food consumption were noted between exposure groups. Exposure paradigm is represented in **Figure 1**. ***Breeding strategy:*** To obtain fetuses, timed matings were carried out by exchanging female and male bedding three days prior to mating, and then pairing 1:1 male:female in the male cage overnight. The next morning was designated GD0.5 (gestational day 0.5) and males were removed to avoid asynchronous pregnancies. Successful pregnancy was confirmed by weight gain. Fetuses were harvested from the first litter of pregnant females euthanized by CO_2 overdose on gestational day (GD) 18. Placenta, lung, liver, and heart tissue were collected from fetuses and flash frozen using liquid nitrogen. ***Sample size:*** The total number of experimental conditions yielded 24 unique samples: 2 different exposure groups (unexposed vs. 100 ppb inorganic arsenic exposed) * 4 different tissues (fetal heart, liver, lung and placenta) * 3 animals per exposure group. Based on prior literature in other comparable studies (Torres, et al., 2016; Vilmundarson et al., 2022), biological triplicates (N=3) for each tissue per exposure group was

determined to be sufficient for the current analysis. Each biological replicate represented a unique litter. ***Randomization:*** fetuses and corresponding placenta were randomly chosen from each litter (n=3 per exposure group) for RNA extraction. Sex as a biological variable was not determined nor considered during the randomization process. ***Inclusion & exclusion criteria:*** Only pregnant females were included in this study to obtain access to fetal tissues. Tissue samples would have been excluded from analysis if contamination occurred or if RNA yield would be less than the 100 ng required for the microarray, or if RNA quality was poor (pure was considered 260/280 ratio >2.0; 2.0 <260/230 ratio< 2.2; and 260/230 ratio > 260/280 ratio). No animals, experimental units, or data points were excluded for this analysis. ***ARRIVE Statement:*** This study was conducted with approval by the Johns Hopkins University Institutional Animal Care and Use Committee (Protocol # MO20H283), following the National Research Council's Guide for the Care and Use of Laboratory Animals. In addition, we have been following the ARRIVE guidelines 2.0 (Percie du Sert 2020) for the entire study.

Total RNA Isolation

Tissues were thawed in RNAprotect (Qiagen Inc., Valencia, CA), ground using frosted slides and run through a Qiashredder column (Qiagen Inc., Valencia, CA) before RNA isolation. Total RNA was extracted from each organ (<30 mg) using RNeasy Mini kits (Qiagen Inc., Valencia, CA). Quantity and purity of total RNA was measured using a Take3 Microvolume Plate and the Take3 app (Agilent Technologies, Santa Clara, CA). Total RNA was considered pure when 260/280 ratio >2.0; 2.0 <260/230 ratio< 2.2; and 260/230 ratio > 260/280 ratio.

RT-qPCR

RT-qPCR was run on a set of samples (N=2-5) using Universal SYBR Green Fast qPCR Mix (Cat no. RK21203; ABClonal Inc., Woburn, MA) and primer sets in the published literature (**Table 1**). All runs were normalized to the 18S ribosomal housekeeping gene (**Table 1**) previously used by Espindola et al. (2012). For proteasome 20S subunit beta 8 (PSMB8), a TaqMan probe was utilized (Cat no. 4453320; Applied Biosystems, Waltham, MA) following instructions from the manufacturer.

Microarray

Total RNA was reverse-transcribed to cDNA using the Applied Biosystems High-Capacity cDNA Reverse Transcription Kit (Cat no. 4368814; Applied Biosystems, Waltham, MA).

Gene expression analysis was carried out using Agilent Whole Mouse 44K Genome Oligo Array (Agilent Technologies) according to manufacturer instructions. Due to poor RNA isolation, the total number of samples included in the final analysis was N=3 per group (arsenic & control).

Statistical Analysis

RT-qPCR results were analyzed using GraphPad Prism 9 (GraphPad Software, Boston, MA). Groups were compared using an ANOVA with post hoc analysis Bartlett's statistic (corrected; for Guanylate-Binding Protein 3) or Tukey's multiple comparisons test (for all others).

Data from microarray experiments were preprocessed using GeneSpring (Agilent Technologies, Santa Clara, CA) software. Raw data were imported and quantile-normalized. Statistical analysis was done using limma with a moderated Bayes t-test and a Benjamini-Hochberg correction. Although no individual gene was statistically significantly changed after correcting for multiple hypothesis testing, all genes with an unadjusted *p*-value less than 0.01 were investigated for further pathway analysis.

Protein-protein Interaction Networks and Pathway Enrichment

We queried over-represented pathways using Search Tool for the Retrieval of Interacting Genes/Proteins (STRING, v12.0, string-db.org), a database that extracts experimental and curated data from several sources to deduce protein-protein interaction (PPI) networks from a set of protein-coding genes (Szklarczyk et al. 2023). Using a differentially expressed genes (DEGs) list cutoff, |log2FC|>0 and adjusted *p*-value cutoff of <0.05, we generated PPI networks for the gene sets for each tissue using the STRING medium confidence required interaction score. When no individual gene was statistically significantly changed after correcting for multiple hypothesis testing, all genes with an uncorrected p-value less than .01 were investigated for over-represented pathways via STRING. These were visualized in STRING with all potential interaction sources used and a moderate level of evidence; enrichment statistics were performed using STRING with the assumption of the whole genome as background. We limited our network generation to only include experimental evidence and evidence from curated databases as active interaction sources. Experimental databases in STRING are (BIND, DIP, GRID, HPRD, IntAct, MINT, and PID), and the curated databases in STRING include the gene ontology (GO) database (Gene Ontology Consortium 2004), KEGG database (Kanehisa and Goto, 2000), Biocarta, BioCyc and Reactome. Finally, Cytoscape (v 3.9.1) (Shannon et al. 2003) an open-source platform, was used to search whether there were any additional pathways.

Results

qRT-PCR Analysis

Selected genes based on prior arsenic exposure literature were analyzed using RT-PCR to examine organ-specific alterations in gene expression following preconception and prenatal arsenic exposure. Although no significance was discovered, there was a trending association in placenta. In the liver, IFITM3 and PSMB8 were unchanged when treatments were compared to controls (**Figure 2, A & B**). Unfortunately, the number of control liver samples were limited in this sample set; therefore, any alterations that may exist could have been clouded by a small sample size. Similarly, in the heart, no significant differences were observed in relative expression of lipoprotein lipase (Lpl) or integrin beta 1 (Itgb1) (**Figure 2, C & D**). One sample in the male arsenic group had higher expression of 18S ribosomal RNA compared to other samples (still within two standard deviations of the mean) which resulted in much higher 2^ΔΔCt values for both heart mRNAs. Nop56 ribonucleoprotein (Nop56) expression in lung tissue was also unaffected by treatment, with some samples showing higher expression than others, but no major trends were observed across treatment groups (**Figure 2E**). Finally, Guanylate-Binding Protein 3 (Gbp3) expression in placenta neared significance when comparing female arsenic-exposed placentas to controls (**Figure 2F**). Arsenic-exposed samples exhibited higher levels of this mRNA (p=0.0762).

Microarray Analysis

Raw data from microarray experiments was preprocessed, quantile-normalized and differential gene expression between exposed (100 ppb iAs) and unexposed (0 ppb) was determined for fetal heart (**Table S1**), liver (**Table S2**), lung (**Table S3**) and placenta (**Table S4**). Of the genes altered with an unadjusted p-value <0.01, just four mapped genes were changed across all tissues: the heart, liver, and placenta (Pim3, Ifit3, Psmb8, and Rtp4; **Figure 3**). Between the heart and liver, overlap occurred in 15 genes: C1qb, Tyrobp, Hic1, Ankrd37, Ly6c1, Gm16430, Isg15, Ifitm3, Gcm1, Irf9, Usp18, Oas1a, Oasl1, Xaf1, and Gzma. Heart and placenta had eight of the same differentially expressed genes (Hmga1, Irgm2, Irgm1,

Tmem140, Pde4b, Ifi204, Gbp3, and Cmpk2). Liver and placenta had just three overlapping genes (Tgtp2, Pfkfb3, and Dek). While 49 genes were found to be differentially expressed in the lung, none overlapped with any of the other organs studied. After the altered genes for each organ were input into STRING and a map was acquired, dysregulated biological pathways were identified.

Fetal Liver: Findings from the liver revealed 251 differentially expressed transcripts, of which 240 were known and could be input into STRING (**Figure 4**). In the microarray, Interferon-induced transmembrane protein 3 (Ifitm3) was downregulated in arsenic-exposed mice (-1.02 log fold change). Interestingly, Ifitm3 and Psmb8 were two of the genes found to be highly connected to other altered transcripts. Enriched biological processes included regulation of biological process, cellular process, and biological regulation (top 10 results in **Table 2**, complete list in **Table S5**). No KEGG pathway enrichment was identified in the STRING database based on the input. After inputting the same differentially expressed transcripts into Cytoscape, the human pathway related to immune response to tuberculosis (WP4197) was identified. In particular, the downstream regulation of this pathway includes PSMB8, IFIT3, and interferon regulatory factors (IRF) 1 & 9, which were found to be differentially regulated in the current mouse model.

Fetal Heart: Data from the heart revealed 163 differentially expressed RNA transcripts, of which 150 known transcripts were entered into STRING. A STRING interaction map was generated (**Figure 5**) and information was obtained on enriched biological processes (based on gene ontology - GO) and KEGG pathways (top 10 STRING/GO findings in **Table 3**, all KEGG findings in **Table 4**). The three most enriched biological processes were immune system process, immune response, and immune effector process. Similarly, enriched KEGG pathways revolved mainly around immune response with the top three as prion diseases, osteoclast differentiation, and the B cell receptor signaling pathway. Again, in the heart, Psmb8 was a highly connected transcript, as was Ifitm3. C-C motif chemokine ligand 5 (Ccl5) appeared to be a key factor linking various components of the two major networks identified in the STRING diagram.

Both Itgb1 and Lpl were slightly outside of the main networks but still connected to many other dysregulated genes. Cytoscape inquiry revealed the human macrophage markers CD68 and coagulation factor 3 (F3) as two of the dysregulated genes related to the WikiPathway WP4146 – Macrophage markers.

Fetal Lung: A total of 49 mRNAs were altered in lung tissue, with 41 of these being input into the STRING program. Nop56 was one of the most connected transcripts identified in the generated STRING map for the lung. Although a small network of genes was identified to be interacting (**Figure 6**), four biological processes were found to be enriched within the set including chromatin assembly, ribosome biogenesis, cellular component biogenesis, and nucleosome assembly (**Table 5A**). Just one KEGG pathway was enriched; cysteine and methionine metabolism (**Table 5B**). Similarly, analysis in Cytoscape mapped DNA methyltransferase 3B (Dnmt3b) and 3-phosphoglycerate dehydrogenase (Phgdh) to WP2525, the pathway for trans-sulfuration and one-carbon metabolism.

Placenta: In the placenta, there were 190 differentially expressed mRNAs; 165 of these were input into STRING because many of them were not mapped to a known transcript. There was one more highly connected area in the STRING map and many of those connections included Gbp3 and Psmb8 (**Figure 7**). Although there were no GO or KEGG pathways found to be enriched in this data, enriched cellular components were identified (**Table 6**). After input into Cytoscape, the same pathway identified for liver tissue exhibited similarity in the dysregulated genes for placenta tissue. Specifically, Ifit3, Psmb8, and protein tyrosine phosphatase, non-receptor type 2 (Ptpn2) mapped to this pathway.

Discussion

Although Ifitm3 was not found to be significantly different in the liver of this model upon examination by RT-PCR, it was one of the most differentially expressed transcripts in the microarray and was highly

connected in the STRING map. Considering that the microarray only included one sample, different to those run with RT-PCR, perhaps that individual was a high expresser for this transcript. However, it reveals that investigation of a single transcript in response to low level arsenic exposure is not sufficient to display a complete portrait of effects. Furthermore, in both the liver and placenta, this dysregulated gene, along with Psmb8, mapped to the pathway involved in immune response to tuberculosis. Ifitm3 normally acts to inhibit viral entry into host cell cytoplasm (Li et al. 2013; Narayana et al. 2015); therefore, as a potential mechanism of immune suppression following prenatal arsenic exposure, it is of interest for further investigation. Ifitm3 was one of just a few genes found to be altered in the heart, liver, and placenta and has been identified as an intrinsic factor which can be upregulated by interferons (Jiang et al. 2018). It is also recognized as a limiting factor in influenza pathogenesis (Everitt et al. 2012) and seems to play a role in human metastasis prevention (Gómez-Herranz et al. 2019). Found to be downregulated in chronically iAs-treated hamsters (Hernández et al. 2011), Ifitm3 was identified as a potential mediator of hepatic carcinogenesis. Despite the fact that the exposure level was significantly higher in the hamsters (15 mg/L or 15,000 ppb), Ifitm3 and related pathways represent potential targets for mechanistic intervention. Furthermore, given the data on long-term susceptibility to tuberculosis following prenatal exposure to arsenic, Ifitm3 and Psmb8 may be mediators, along with other intrinsic factors, of those long-term effects.

Psmb8, or proteasome 20S subunit beta 8, is a key component of MHC class II and is expressed in many tissues in the body (PubChem). It is induced by interferon gamma and, interestingly, mutation in this subunit of the immunoproteasome has been linked to increased inflammation and lipodystrophy (Kitamura et al. 2011). Results from the current inquiry reveal a small downregulation of Psmb8 in the placenta, heart, and liver. Prior work found no effect of arsenic trioxide on expression of Psmb8 in NB4 acute promyelocytic leukemia cells; however, in the same study, a reduction in promoter activity of Psmb8 was noted (Yang et al. 2014).

Despite setting out to discover the relationship between prenatal arsenic exposure and the glucocorticoid receptor signaling pathway, the results highlight the known link between arsenic and impaired lipid metabolism (Renu et al. 2018), which is, of course, also linked to macrophage function. Nop56, found to be dysregulated in the lung of this model, has previously been found to be associated with metal exposure (including arsenic) and atherosclerosis (Riffo-Campos et al. 2018). Prenatal exposure has previously been linked to altered signaling in the liver, contributing to earlier onset of atherosclerosis in the apolipoprotein E-knockout mouse model (States et al. 2012). Lpl encodes a water-soluble enzyme important in lipoprotein processing, an essential macrophage function. It was not found to be different after RT-PCR analysis, but was identified as an altered transcript in the microarray. Interestingly, Lpl was found to be down-regulated following arsenic exposure due to its suppressive effect (arguably, toxicity) to macrophages (Song et al. 2019). Interestingly, recent work has shown that a drug inhibiting lipase activity can reverse these effects (Lou et al. 2022).

Other findings were less specific but many still are related to the immune response. For instance, Itgb1, involved in cell adhesion and recognition for multiple processes including immune response, did not show significant differences in RT-PCR analysis but exhibited altered expression in the microarray results. Further, this member of the arrestin family of proteins was found to be positively associated with arsenic exposure in two Bangladeshi cohorts (Demanelis et al. 2019). Gbp3 (-0.43 log FC), a transcript previously found to be upregulated in arsenic-exposed fetal C3H mouse liver (Liu et al. 2007), is one of a group of GTPases upregulated in response to interferons. Evidence indicates that this variant acts to moderate influenza virus, decreasing viral activity within the cell (Nordmann et al. 2012). In this study, a decrease in Gbp3 was observed in the placenta and liver, in alignment with findings of larger immune pathway downregulation and increased susceptibility to respiratory infection observed in human populations following prenatal arsenic exposure (Farzan et al. 2016; Laine and Fry 2016).

Importantly, these findings underline the idea that although small changes may be observed in individual genes across organs, these minute alterations across a network can lead to larger ramifications at the system level. This idea of network dynamics is influencing the field of medicine and allowing for use of artificial intelligence in order to make predictions about disease and treatment based on transcriptomic data (Theodoris et al. 2023). Using the presented data, a comparison across organs, in conjunction with other studies allows for correlation and furthers understanding of the mechanistic basis for long-term effects of preconception and prenatal arsenic exposure.

To our knowledge this is the first publication making a comparison of gene expression alterations in multiple organs following prenatal exposure to a relevant level of arsenic. Further investigation into these pathways as potential mechanistic targets to prevent long-term effects of arsenic exposure is needed.

COI: The authors claim no conflict of interest.

Funding Statement: This work was supported by the National Institutes of Health Grants NIEHS - R00ES024808 (F.S.), NIEHS - T32ES07141 (K.A.R., and E.I.), and NHLBI 5T32HL007534-35 (S.S.).

Acknowledgements: We acknowledge Tyrone Howard for his assistance with animal care and tissue collections. We acknowledge Vy Tran for help with the data analysis. K.A.R. was affiliated with the Department of Environmental Health and Engineering, Bloomberg School of Public Health, Johns Hopkins University at the time of the research and is currently affiliated with the School of Health Professions, University of Mary Hardin-Baylor.

Tables & Figures

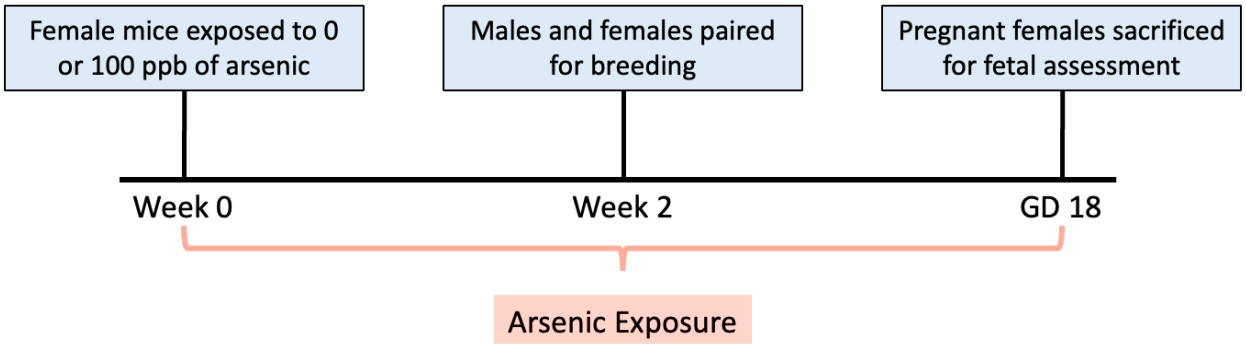

Figure 1. Preconception and prenatal arsenic exposure paradigm. C57Bl/6J mice were exposed to either 0 ppb (control) or 100 ppb (exposed) sodium (meta) arsenite (iAs) in drinking water from two weeks prior to breeding until euthanasia of the pregnant dam at gestational day (GD) 18. Samples were collected at GD 18 including liver, heart, lung, and placenta and flash frozen using liquid nitrogen.

Gene	Forward	Reverse
IFITM3	CTGAACATCAGCACCTTGGT	TTTTGGTGGTTATCAAGTGCACT
Lpl	GTGGCCGAGAGCGAGAACAT	GCTTTCACTCGCATCCTCTC
Itgb1	TGTGACCCATTGCAAGGAGAAGGA	AATTGGGATGATGTCGGGACCAGT
Nop56	GTTGGCGCTGAAGGAAGTGG	CTTTGGCACGAGAGTAGCTG
Gbp3	TGGAGGCACCCATTTGTCTGGTG	GACAAAGGTGCTGCTCAGAAGCACAG
18S	GGGAGCCTGAGAAACGGC	GGGTCGGGAGTGGGTAATTT

Table 1. Primer sets for RT-qPCR. The primer sets listed in the table were utilized for analysis of mRNA for individual genes selected from the most dysregulated genes from the microarray data that demonstrated the most connections in generated STRING maps. All mRNA quantification was normalized to 18S ribosomal mRNA expression.

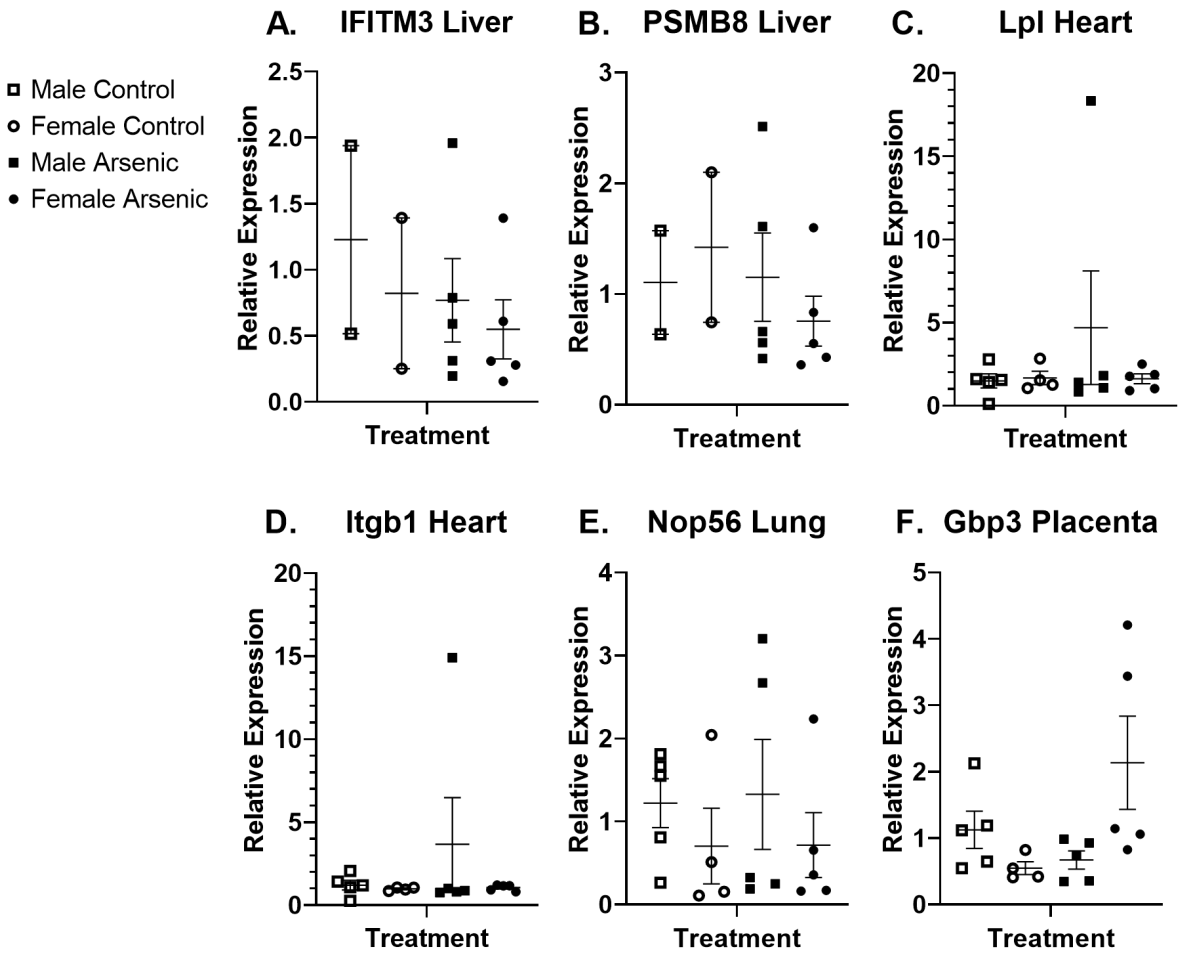

Figure 2. RT-qPCR Analysis of Select Genes in Lung, Liver, Heart, and Placenta of GD18 mice offspring prenatally exposed to arsenic. Tissues including heart, lung, liver, and placenta were excised upon euthanasia of the pregnant dam at gestational day (GD) 18 following preconception and prenatal exposure to either 0 ppb (control) or 100 ppb (exposed) sodium (meta) arsenite. Tissues from the C57Bl/6J mice were flash frozen using liquid nitrogen and stored at -80˚ C. RNA was extracted using Qiagen kits, reverse transcribed, and gene expression analysis was carried out using RT-qPCR. Select genes (IFITM3 and PSMB8 in liver, Lpl and Itgb1 in heart, Nop56 in lung, and Gbp3 in placenta) were

analyzed by RT-qPCR to examine organ-specific alterations in gene expression. All runs were normalized to 18S ribosomal RNA. N=2-5 from at least two litters. No findings reached statistical significance.

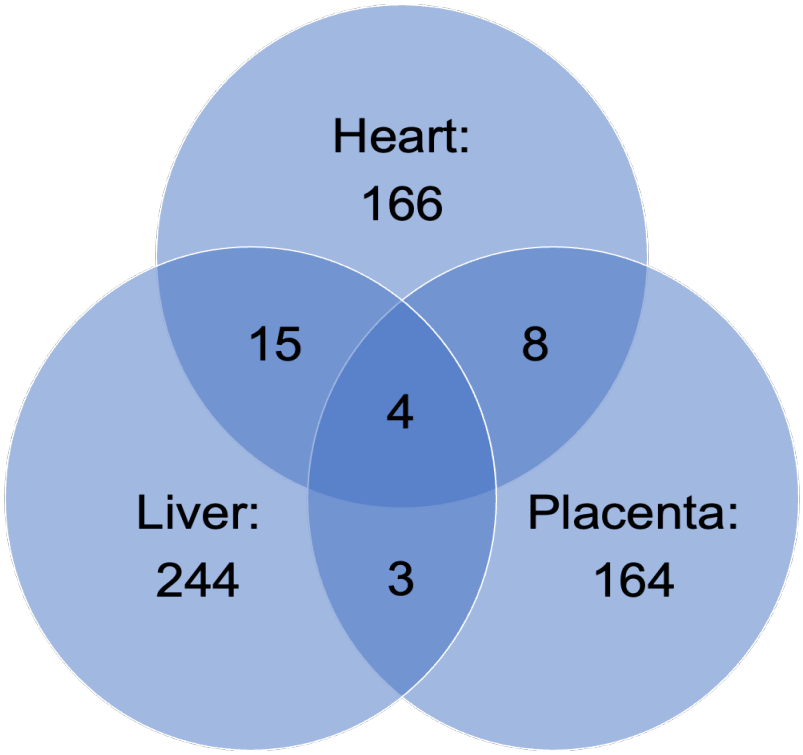

Figure 3. Differential gene expression overlap between heart, liver, and placenta. Tissues including heart, lung, liver, and placenta were excised upon euthanasia of the pregnant dam at gestational day (GD) 18 following preconception and prenatal exposure to either 0 ppb (control) or 100 ppb (exposed) sodium (meta) arsenite. Tissues from the C57Bl/6J mice were flash frozen using liquid nitrogen and stored at -80˚ C. RNA was extracted using kits from Qiagen, reverse transcribed, and gene expression analysis was carried out using the Agilent Whole Mouse 44K Genome Oligo Array. Among the genes altered with an unadjusted *p*-value <0.01, only four were found to overlap between placenta, liver, and heart. Similarly, there was minimal overlap between heart and liver (15), liver and placenta (3), and

heart and placenta (8). No overlapping genes were identified between the lung and any other organ. Data shown represents an N=3.

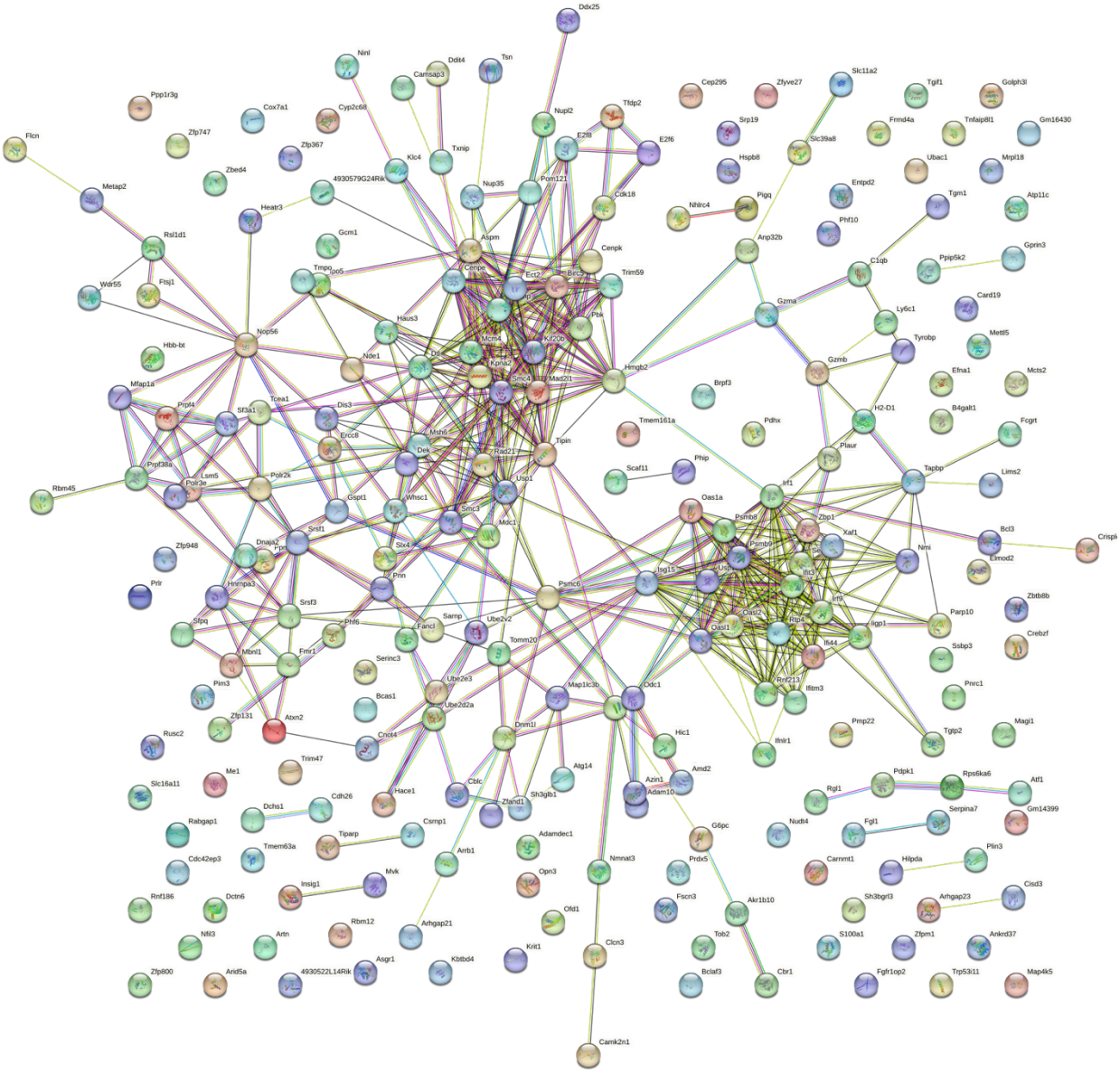

Figure 4. Liver STRING Map. Liver samples were obtained from gestational day (GD) 18 C57Bl/6J fetal mice exposed for 2 weeks prior to conception and during gestation to either 0 ppb (control) or 100 ppb (exposed) sodium (meta) arsenite. After microarray analysis, 240 differentially expressed (comparing exposed to controls exhibited an unadjusted *p*-value <0.01) genes from the liver were entered into the

STRING database to generate a map. Nodes are indicated by the colored circles; lines indicate connections between nodes. Data shown represents an N=3.

GO Term ID	Term Description	Observed Gene Count	Background Gene Count	Strength	False Discovery Rate	Matching Proteins in Your Network (Labels)
GO:0050789	Regulation of biological process	163	9973	0.18	1.95E-08	Plaur,Tmem161a,Fancl,Clcn3,Brpf3,Msh6,Gzmb,Serinc3,Pmp22,Kpna2,G6pc,Plin3,Tmpo,Ddit4,Ppm1d,E2f6,Dek,Cenpk,Psmc6,Pbk,Rad21,Atf1,Slc11a2,Gzma,Gcm1,Phf10,Tapbp,Psmb8,Lims2,Incenp,Prdx5,Smc3,Ifitm3,Cdk18,Rgl1,Opn3,Dtl,Entpd2,Nup35,Ube2e3,Zbp1,Efna1,B4galt1,Usp1,Ssbp3,Sfpq,Oasl1,Oasl2,Usp18,Iigp1,Tyrobp,Ipo5,Serpina7,Fgl1,Map1lc3b,Ddx25,Phip,Tipin,Me1,Csrnp1,Mvk,Hspb8,Zfand1,Slx4,Atg14,Hace1,Serpine1,Cblc,C1qb,Ofd1,Pim3,Card19,Tiparp,Rbm12,Zfp367,Elmod2,Hic1,Atxn2,E2f8,Cenpe,Zfpm1,S100a1,Whsc1,Aspm,Ercc8,Camk2n1,Hilpda,Tob2,Insig1,Adam10,Artn,Nfil3,Azin1,Hmgb2,Ly6c1,Cdc42ep3,Ifnlr1,Frmd4a,Tnfaip8l1,Dchs1,Phf6,Gspt1,Krit1,Birc5,Oas1a,Slc39a8,Rps6ka6,Isg15,Kif20b,Fmr1,Magi1,Rnf213,Hbb-bt,Arrb1,Cox7a1,Mbnl1,Mad2l1,Atp11c,Flcn,Ifit3,Anp32b,Pdpk1,Sirt1,Zbtb8b,Txnip,Crebzf,Trim59,Ect2,Irf1,Map4k5,Hnrnpa3,Bclaf3,Cnot4,Arid5a,Dnm1l,Ube2v2,Rnf186,Arhgap23,Rsl1d1,Bcl3,Srsf3,Irf9,Srsf1,Nmi,Prlr,Ppp1r3g,Xaf1,Cep295,Camsap3,Lsm5,Tgm1,Tfdp2,Odc1,Tcea1,Parp10,Sh3glb1,Zfyve27,Tgif1,Psmb9,Arhgap21,H2-D1,Golph3l,Zfp131
GO:0009987	Cellular process	195	13330	0.13	2.93E-08	Sf3a1,Plaur,Tmem161a,Fancl,Clcn3,Brpf3,Msh6,Pdhx,Bcas1,Gzmb,Serinc3,Pmp22,Kpna2,G6pc,Nudt4,Ddit4,Ppm1d,E2f6,Trim47,Pnn,Dek,Cenpk,Psmc6,Pbk,Rad21,Mcm4,Nde1,Atf1,Slc11a2,Gzma,Gcm1,Phf10,Tapbp,Psmb8,Lims2,Incenp,Carnmt1,Prdx5,Smc3,Ifitm3,Pigq,Tsn,Cdk18,Rgl1,Tmem63a,Opn3,Dtl,Entpd2,Nup35,Ube2e3,Zbp1,Efna1,B4galt1,Usp1,Ssbp3,Sfpq,Sh3bgrl3,Oasl2,Fscn3,Usp18,Iigp1,Tyrobp,Ipo5,Polr3e,Dctn6,Fgl1,Heatr3,Dnaja2,Map1lc3b,Ddx25,Phip,Tipin,Me1,Csrnp1,Mvk,Hspb8,Zfand1,Slx4,Wdr55,Atg14,Hace1,Serpine1,Cblc,Ubac1,C1qb,Rbm45,Rtp4,Ofd1,Dis3,Pim3,Smc4,Tiparp,Cdh26,Cbr1,Haus3,Mettl5,Polr2k,Hic1,Atxn2,E2f8,Cenpe,Zfpm1,Whsc1,Aspm,Ercc8,Hilpda,Insig1,Nupl2,Adam10,Artn,Nfil3,Azin1,Hmgb2,Ly6c1,Cdc42ep3,Rabgap1,Srp19,Ifnlr1,Frmd4a,Dchs1,Mrpl18,Prpf38a,Gspt1,Krit1,Birc5,Oas1a,Amd2,Slc39a8,Rps6ka6,Mdc1,Prpf4,Nhlrc4,Isg15,Kif20b,Fmr1,Magi1,Mfap1a,Asgr1,Rnf213,Hbb-bt,Arrb1,Cox7a1,Mbnl1,Mad2l1,Atp11c,Nop56,Flcn,Ifit3,Anp32b,Pdpk1,Mcts2,Sirt1,Txnip,Crebzf,Trim59,Ect2,Irf1,Ninl,Map4k5,Pom121,Hnrnpa3,Ppip5k2,Nmnat3,Cnot4,Arid5a,Dnm1l,Ube2v2,Rnf186,Arhgap23,Rsl1d1,Bcl3,Slc16a11,Srsf3,Srsf1,Nmi,Prlr,Crispld2,Xaf1,Camsap3,Lsm5,Tgm1,Tfdp2,Odc1,Tcea1,Parp10,Sh3glb1,Zfyve27,Tgif1,Ube2d2a,Psmb9,Arhgap21,H2-D1,Golph3l,Tomm20,Metap2
GO:0065007	Biological regulation	167	10591	0.16	6.45E-08	Plaur,Tmem161a,Fancl,Clcn3,Brpf3,Msh6,Gzmb,Serinc3,Pmp22,Kpna2,G6pc,Plin3,Tmpo,Ddit4,Ppm1d,E2f6,Dek,Cenpk,Psmc6,Pbk,Rad21,Nde1,Atf1,Slc11a2,Gzma,Gcm1,Phf10,Tapbp,Psmb8,Lims2,Incenp,Prdx5,Smc3,Ifitm3,Cdk18,Rgl1,Opn3,Dtl,Entpd2,Nup35,Ube2e3,Zbp1,Efna1,B4galt1,Usp1,Ssbp3,Sfpq,Oasl1,Oasl2,Usp18,Iigp1,Tyrobp,Ipo5,Serpina7,Fgl1,Dnaja2,Map1lc3b,Ddx25,Phip,Tipin,Me1,Csrnp1,Mvk,Hspb8,Zfand1,Slx4,Atg14,Hace1,Serpine1,Cblc,C1qb,Ofd1,Dis3,Pim3,Card19,Tiparp,Rbm12,Zfp367,Elmod2,Hic1,Atxn2,E2f8,Cenpe,Zfpm1,S100a1,Whsc1,Aspm,Ercc8,Camk2n1,Hilpda,Tob2,Insig1,Adam10,Artn,Nfil3,Azin1,Hmgb2,Ly6c1,Cdc42ep3,Rabgap1,Ifnlr1,Frmd4a,Tnfaip8l1,Dchs1,Phf6,Gspt1,Krit1,Birc5,Oas1a,Slc39a8,Rps6ka6,Isg15,Kif20b,Fmr1,Magi1,Rnf213,Hbb-bt,Arrb1,Cox7a1,Mbnl1,Mad2l1,Atp11c,Flcn,Ifit3,Anp32b,Pdpk1,Sirt1,Zbtb8b,Txnip,Crebzf,Trim59,Ect2,Irf1,Map4k5,Hnrnpa3,Bclaf3,Cnot4,Arid5a,Dnm1l,Ube2v2,Rnf186,Arhgap23,Rsl1d1,Bcl3,Srsf3,Irf9,Srsf1,Nmi,Prlr,Ppp1r3g,Xaf1,Cep295,Camsap3,Lsm5,Tgm1,Tfdp2,Odc1,Tcea1,Parp10,Sh3glb1,Zfyve27,Tgif1,Psmb9,Arhgap21,H2-D1,Golph3l,Zfp131
GO:0019222	Regulation of metabolic process	115	6085	0.24	7.81E-08	Plaur,Tmem161a,Clcn3,Brpf3,Msh6,Pmp22,G6pc,Tmpo,Ddit4,Ppm1d,E2f6,Dek,Cenpk,Psmc6,Pbk,Rad21,Atf1,Slc11a2,Gzma,Gcm1,Phf10,Tapbp,Psmb8,Incenp,Prdx5,Smc3,Cdk18,Dtl,Nup35,Efna1,Usp1,Ssbp3,Sfpq,Oasl1,Oasl2,Iigp1,Tyrobp,Serpina7,Fgl1,Ddx25,Phip,Tipin,Me1,Csrnp1,Mvk,Hspb8,Slx4,Atg14,Hace1,Serpine1,Cblc,Tiparp,Rbm12,Zfp367,Hic1,Atxn2,E2f8,Cenpe,Zfpm1,S100a1,Whsc1,Ercc8,Camk2n1,Hilpda,Tob2,Insig1,Nfil3,Azin1,Hmgb2,Phf6,Gspt1,Birc5,Oas1a,Slc39a8,Rps6ka6,Isg15,Fmr1,Hbb-bt,Arrb1,Cox7a1,Mbnl1,Mad2l1,Flcn,Anp32b,Pdpk1,Sirt1,Zbtb8b,Txnip,Crebzf,Ect2,Irf1,Map4k5,Hnrnpa3,Bclaf3,Arid5a,Dnm1l,Ube2v2,Bcl3,Srsf3,Irf9,Srsf1,Nmi,Prlr,Ppp1r3g,Cep295,Camsap3,Lsm5,Tfdp2,Odc1,Tcea1,Parp10,Sh3glb1,Tgif1,Psmb9,Zfp131
GO:0060255	Regulation of macromolecule metabolic process	107	5618	0.24	3.81E-07	Plaur,Tmem161a,Brpf3,Msh6,Pmp22,G6pc,Tmpo,Ddit4,Ppm1d,E2f6,Dek,Cenpk,Psmc6,Pbk,Rad21,Atf1,Slc11a2,Gzma,Gcm1,Phf10,Tapbp,Psmb8,Incenp,Prdx5,Smc3,Cdk18,Dtl,Nup35,Efna1,Usp1,Ssbp3,Sfpq,Oasl1,Oasl2,Tyrobp,Serpina7,Ddx25,Phip,Tipin,Csrnp1,Mvk,Slx4,Atg14,Hace1,Serpine1,Cblc,Tiparp,Rbm12,Zfp367,Hic1,Atxn2,E2f8,Cenpe,Zfpm1,S100a1,Whsc1,Ercc8,Camk2n1,Hilpda,Tob2,Insig1,Nfil3,Azin1,Hmgb2,Phf6,Gspt1,Birc5,Oas1a,Slc39a8,Rps6ka6,Isg15,Fmr1,Hbb-bt,Arrb1,Mbnl1,Mad2l1,Flcn,Anp32b,Pdpk1,Sirt1,Zbtb8b,Txnip,Crebzf,Ect2,Irf1,Map4k5,Hnrnpa3,Bclaf3,Arid5a,Dnm1l,Ube2v2,Bcl3,Srsf3,Irf9,Srsf1,Nmi,Prlr,Ppp1r3g,Cep295,Lsm5,Tfdp2,Odc1,Tcea1,Parp10,Tgif1,Psmb9,Zfp131
GO:0031323	Regulation of cellular metabolic process	103	5479	0.24	1.94E-06	Plaur,Tmem161a,Clcn3,Brpf3,Msh6,Pmp22,Tmpo,Ddit4,Ppm1d,E2f6,Dek,Cenpk,Psmc6,Pbk,Rad21,Atf1,Slc11a2,Gzma,Gcm1,Phf10,Incenp,Prdx5,Smc3,Cdk18,Nup35,Efna1,Usp1,Ssbp3,Sfpq,Oasl1,Oasl2,Iigp1,Tyrobp,Serpina7,Fgl1,Ddx25,Phip,Tipin,Csrnp1,Mvk,Hspb8,Slx4,Atg14,Serpine1,Cblc,Rbm12,Zfp367,Hic1,Atxn2,E2f8,Cenpe,Zfpm1,S100a1,Whsc1,Ercc8,Camk2n1,Tob2,Insig1,Nfil3,Hmgb2,Phf6,Gspt1,Birc5,Oas1a,Slc39a8,Rps6ka6,Isg15,Fmr1,Hbb-bt,Arrb1,Cox7a1,Mbnl1,Mad2l1,Flcn,Anp32b,Pdpk1,Sirt1,Zbtb8b,Txnip,Crebzf,Ect2,Irf1,Map4k5,Hnrnpa3,Bclaf3,Arid5a,Dnm1l,Ube2v2,Bcl3,Srsf3,Irf9,Srsf1,Nmi,Prlr,Ppp1r3g,Cep295,Camsap3,Tfdp2,Tcea1,Parp10,Sh3glb1,Tgif1,Zfp131
GO:0050794	Regulation of cellular process	151	9541	0.16	1.94E-06	Plaur,Tmem161a,Fancl,Clcn3,Brpf3,Msh6,Gzmb,Serinc3,Pmp22,Kpna2,Tmpo,Ddit4,Ppm1d,E2f6,Dek,Cenpk,Psmc6,Pbk,Rad21,Atf1,Slc11a2,Gzma,Gcm1,Phf10,Incenp,Prdx5,Cdk18,Dtl,Nup35,Efna1,Usp1,Ssbp3,Sfpq,Oasl1,Oasl2,Iigp1,Tyrobp,Ipo5,Serpina7,Fgl1,Ddx25,Phip,Tipin,Csrnp1,Mvk,Hspb8,Slx4,Atg14,Hace1,Serpine1,Cblc,Ofd1,Pim3,Card19,Tiparp,Rbm12,Zfp367,Hic1,Atxn2,E2f8,Cenpe,Zfpm1,S100a1,Whsc1,Aspm,Ercc8,Camk2n1,Hilpda,Tob2,Insig1,Adam10,Artn,Nfil3,Azin1,Hmgb2,Ly6c1,Cdc42ep3,Ifnlr1,Frmd4a,Tnfaip8l1,Dchs1,Phf6,Gspt1,Krit1,Birc5,Oas1a,Slc39a8,Rps6ka6,Isg15,Kif20b,Fmr1,Magi1,Rnf213,Hbb-bt,Arrb1,Cox7a1,Mbnl1,Mad2l1,Atp11c,Flcn,Ifit3,Anp32b,Pdpk1,Sirt1,Zbtb8b,Txnip,Crebzf,Trim59,Ect2,Irf1,Map4k5,Hnrnpa3,Bclaf3,Cnot4,Arid5a,Dnm1l,Ube2v2,Rnf186,Arhgap23,Rsl1d1,Bcl3,Srsf3,Irf9,Srsf1,Nmi,Prlr,Ppp1r3g,Xaf1,Cep295,Camsap3,Tgm1,Tfdp2,Odc1,Tcea1,Parp10,Sh3glb1,Zfyve27,Tgif1,Arhgap21,H2-D1,Golph3l,Zfp131
GO:0080090	Regulation of primary metabolic process	100	5290	0.24	2.46E-06	Plaur,Tmem161a,Msh6,Pmp22,Tmpo,Ddit4,Ppm1d,E2f6,Dek,Cenpk,Psmc6,Pbk,Rad21,Atf1,Slc11a2,Gzma,Gcm1,Phf10,Psmb8,Incenp,Prdx5,Cdk18,Dtl,Nup35,Efna1,Usp1,Ssbp3,Sfpq,Oasl1,Oasl2,Serpina7,Fgl1,Ddx25,Phip,Csrnp1,Mvk,Slx4,Atg14,Hace1,Serpine1,Cblc,Tiparp,Rbm12,Zfp367,Hic1,E2f8,Cenpe,Zfpm1,S100a1,Whsc1,Ercc8,Camk2n1,Tob2,Insig1,Nfil3,Azin1,Hmgb2,Phf6,Gspt1,Birc5,Oas1a,Slc39a8,Rps6ka6,Isg15,Fmr1,Hbb-bt,Arrb1,Mbnl1,Mad2l1,Flcn,Anp32b,Pdpk1,Sirt1,Zbtb8b,Txnip,Crebzf,Ect2,Irf1,Map4k5,Hnrnpa3,Bclaf3,Arid5a,Dnm1l,Ube2v2,Bcl3,Srsf3,Irf9,Srsf1,Nmi,Prlr,Ppp1r3g,Cep295,Tfdp2,Odc1,Tcea1,Parp10,Sh3glb1,Tgif1,Psmb9,Zfp131
GO:0009615	Response to virus	17	235	0.82	3.28E-06	Serinc3,Ddit4,Ifitm3,Zbp1,Oasl1,Oasl2,Polr3e,Rtp4,Ifnlr1,Oas1a,Isg15,Fmr1,Ifit3,Crebzf,Irf1,Bcl3,Odc1
GO:0051171	Regulation of nitrogen compound metabolic process	97	5126	0.24	4.02E-06	Plaur,Tmem161a,Msh6,Pmp22,Tmpo,Ddit4,Ppm1d,E2f6,Dek,Cenpk,Psmc6,Pbk,Rad21,Atf1,Slc11a2,Gzma,Gcm1,Phf10,Psmb8,Incenp,Prdx5,Cdk18,Dtl,Nup35,Efna1,Usp1,Ssbp3,Sfpq,Oasl1,Oasl2,Serpina7,Ddx25,Phip,Csrnp1,Mvk,Slx4,Atg14,Hace1,Serpine1,Cblc,Tiparp,Rbm12,Zfp367,Hic1,E2f8,Cenpe,Zfpm1,S100a1,Whsc1,Ercc8,Camk2n1,Tob2,Insig1,Nfil3,Azin1,Hmgb2,Phf6,Gspt1,Birc5,Oas1a,Slc39a8,Rps6ka6,Isg15,Fmr1,Hbb-bt,Arrb1,Mbnl1,Mad2l1,Flcn,Anp32b,Pdpk1,Sirt1,Zbtb8b,Txnip,Crebzf,Ect2,Irf1,Map4k5,Hnrnpa3,Bclaf3,Arid5a,Dnm1l,Ube2v2,Bcl3,Srsf3,Irf9,Srsf1,Nmi,Prlr,Cep295,Tfdp2,Odc1,Tcea1,Parp10,Tgif1,Psmb9,Zfp131

Table 2. Top 10 Enriched Biological Processes in arsenic-exposed GD18 Liver Tissue. Along with generation of the STRING map, enriched biological processes were identified based on the 240 differentially expressed (comparing exposed to controls exhibited an unadjusted *p*-value <0.01) genes from the liver using gene ontology (GO). The specific GO number is reported along with its term description. Each protein from the differentially expressed input that are associated with that biological process are listed in the right column of the table. Data shown represents an N=3.

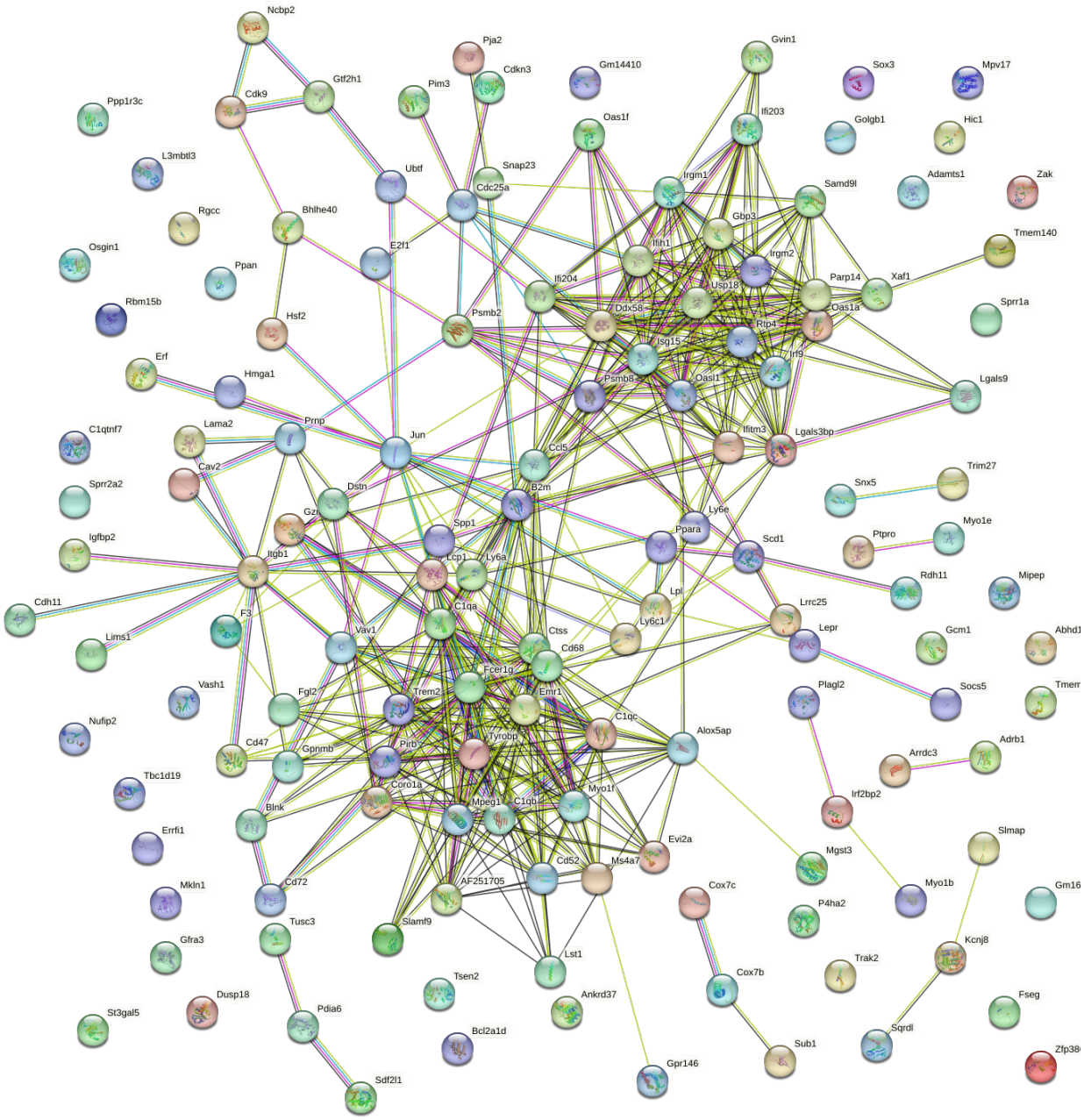

Figure 5. Heart STRING Map. Heart samples were obtained from gestational day (GD) 18 C57Bl/6J fetal mice exposed for 2 weeks prior to conception and during gestation to either 0 ppb (control) or 100 ppb (exposed) sodium (meta) arsenite. After microarray analysis, 156 differentially expressed (comparing exposed to controls exhibited an unadjusted *p*-value <0.01) genes from the heart were entered into the

STRING database to generate a map. Nodes are indicated by the colored circles; lines indicate connections between nodes. Data shown represents an N=3.

# Term ID	Term Description	Observed Gene Count	Background Gene Count	Strength	False Discovery Rate	Matching Proteins In Your Network (Labels)
GO:0002376	immune system process	45	1703	0.58	7.58E-12	Ebi3,Vav1,Ctss,Trim27,Rgcc,Trem2,Psmb8,Ifitm3,Ifih1,Oasl1,Kcnj8,Tyrobp,Coro1a,Myo1e,C1qc,Lepr,L3mbtl3,Parp14,Ccl5,C1qb,Rtp4,Ddx58,C1qa,Irgm1,Blnk,Ptpro,Pirb,Fcer1g,Oas1a,Isg15,Emr1,Myo1f,Itgb1,AF251705,Lst1,B2m,Cd47,Gbp3,Jun,Lgals9,Spp1,Snap23,Samd9l,Lcp1,Pja2
GO:0006955	immune response	30	914	0.68	2.33E-09	Vav1,Ctss,Trim27,Rgcc,Trem2,Ifitm3,Ifih1,Oasl1,Tyrobp,Coro1a,C1qc,Parp14,Ccl5,C1qb,Ddx58,C1qa,Irgm1,Blnk,Pirb,Fcer1g,Oas1a,Isg15,Emr1,Myo1f,Lst1,B2m,Gbp3,Snap23,Lcp1,Pja2
GO:0002252	immune effector process	20	395	0.87	8.36E-09	Rgcc,Ifitm3,Ifih1,Oasl1,Kcnj8,Tyrobp,Coro1a,C1qc,C1qb,Rtp4,Ddx58,C1qa,Pirb,Fcer1g,Oas1a,Isg15,Myo1f,Cd47,Snap23,Lcp1
GO:0050896	response to stimulus	86	6616	0.28	8.36E-09	Cav2,Ebi3,Ppan,Vav1,Gtf2h1,Cdk9,Ctss,Lpl,Lims1,Vash1,Trim27,Rgcc,Sub1,Sdf2l1,Trem2,Gfra3,Ifitm3,Mgst3,Ifih1,F3,Psmb2,Errfi1,Oasl1,Gpnmb,Bhlhe40,Usp18,Kcnj8,Tyrobp,Coro1a,Myo1e,C1qc,Scd1,Lepr,Parp14,Socs5,Ccl5,C1qb,Adrb1,Rtp4,Ddx58,Igfbp2,C1qa,Irgm1,Pdia6,Hic1,Ly6e,Dusp18,Blnk,Cdkn3,Alox5ap,Ptpro,Pirb,Fcer1g,Oas1a,Isg15,Emr1,Myo1f,Itgb1,Zak,Prnp,Lama2,Cdc25a,Lst1,Gpr146,E2f1,B2m,Cd47,Gbp3,Jun,Sprr2a2,Lgals9,Cd68,Ube2v1,Ppara,Ifi204,Spp1,Snap23,Hmga1,Mpv17,Lcp1,Ifi203,Xaf1,Rdh11,Ubtf,Pja2,Ly6a
GO:0051707	response to other organism	29	1050	0.6	1.27E-07	Trim27,Trem2,Ifitm3,Ifih1,Oasl1,Usp18,Kcnj8,Coro1a,C1qc,Scd1,Parp14,Ccl5,C1qb,Rtp4,Ddx58,C1qa,Irgm1,Fcer1g,Oas1a,Isg15,Myo1f,B2m,Cd47,Gbp3,Jun,Lgals9,Ifi204,Pja2,Ly6a
GO:0009605	response to external stimulus	40	2021	0.46	3.18E-07	Ppan,Vav1,Trim27,Trem2,Gfra3,Ifitm3,Ifih1,Oasl1,Bhlhe40,Usp18,Kcnj8,Coro1a,C1qc,Scd1,Parp14,Ccl5,C1qb,Adrb1,Rtp4,Ddx58,Igfbp2,C1qa,Irgm1,Ptpro,Fcer1g,Oas1a,Isg15,Myo1f,Lama2,B2m,Cd47,Gbp3,Jun,Lgals9,Ppara,Ifi204,Spp1,Rdh11,Pja2,Ly6a
GO:0006950	response to stress	49	2899	0.39	3.97E-07	Gtf2h1,Cdk9,Lpl,Vash1,Trim27,Rgcc,Sdf2l1,Trem2,Ifitm3,Ifih1,F3,Errfi1,Oasl1,Kcnj8,Coro1a,C1qc,Scd1,Parp14,Socs5,Ccl5,C1qb,Adrb1,Rtp4,Ddx58,C1qa,Irgm1,Pdia6,Hic1,Cdkn3,Alox5ap,Fcer1g,Oas1a,Isg15,Myo1f,Zak,Prnp,E2f1,B2m,Gbp3,Jun,Ube2v1,Ppara,Ifi204,Spp1,Snap23,Hmga1,Mpv17,Lcp1,Pja2
GO:0050789	regulation of biological process	103	9594	0.19	4.68E-07	Cav2,Ebi3,Ppan,Vav1,Gtf2h1,Cdk9,Ctss,Lpl,Lims1,Vash1,Trim27,Rgcc,Sub1,Sdf2l1,Ncbp2,Adamts1,Gzma,Gcm1,Trem2,Psmb8,Gfra3,Ifitm3,Mkln1,Ifih1,F3,Zfp593,Errfi1,Oasl1,Gpnmb,Bhlhe40,Usp18,Kcnj8,Tyrobp,Coro1a,Myo1e,C1qc,Scd1,Lepr,L3mbtl3,Parp14,Socs5,Ccl5,C1qb,Adrb1,Erf,Ddx58,Pim3,Igfbp2,C1qa,Irgm1,Pdia6,Hic1,Ly6e,Dusp18,Blnk,Rbm15b,Irf2bp2,Fseg,Cdkn3,Alox5ap,Ptpro,Pirb,Hsf2,Fcer1g,Oas1a,Isg15,Emr1,Ppp1r3c,Myo1f,Itgb1,Zak,Prnp,AF251705,Lama2,Cdc25a,Lst1,Arrdc3,Gpr146,E2f1,Dstn,B2m,Cd47,Jun,Lgals9,Ube2v1,Ppara,Papola,Snx5,Ifi204,Spp1,Snap23,Samd9l,Hmga1,Sox3,Mpv17,Lcp1,Slmap,Irf9,Ifi203,Xaf1,Rdh11,Ubtf,Pja2
GO:0006952	defense response	27	1079	0.56	2.09E-06	Trim27,Trem2,Ifitm3,Ifih1,F3,Oasl1,Kcnj8,Coro1a,C1qc,Scd1,Parp14,Ccl5,C1qb,Rtp4,Ddx58,C1qa,Irgm1,Alox5ap,Fcer1g,Oas1a,Isg15,Myo1f,B2m,Gbp3,Jun,Snap23,Pja2
GO:0098542	defense response to other organism	22	735	0.64	2.59E-06	Trim27,Trem2,Ifitm3,Ifih1,Oasl1,Kcnj8,Coro1a,C1qc,Scd1,Parp14,Ccl5,C1qb,Rtp4,Ddx58,C1qa,Irgm1,Fcer1g,Oas1a,Isg15,Myo1f,Gbp3,Pja2

Table 3. Top 10 Enriched Biological Processes in arsenic-exposed GD18 Heart Tissue. Along with generation of the STRING map, enriched biological processes were identified based on the 150 differentially expressed (comparing exposed to controls exhibited an unadjusted *p*-value <0.01) genes from the heart using gene ontology (GO). The specific GO number is reported along with its term description. Each protein from the differentially expressed input that are associated with that biological process are listed in the right column of the table. Data shown represents an N=3.

# Term ID	Term Description	Observed Gene Count	Background Gene Count	Strength	False Discovery Rate	Matching Proteins In Your Network (Labels)
mmu05020	Prion diseases	5	34	1.33	0.001	C1qc,Ccl5,C1qb,C1qa,Prnp
mmu04380	Osteoclast differentiation	6	122	0.85	0.012	Trem2,Tyrobp,Blnk,Pirb,Jun,Irf9
mmu04662	B cell receptor signaling pathway	5	69	1.02	0.012	Vav1,Cd72,Blnk,Pirb,Jun
mmu05133	Pertussis	5	74	0.99	0.012	C1qc,C1qb,C1qa,Itgb1,Jun
mmu05142	Chagas disease (American trypanosomiasis)	5	101	0.86	0.0254	C1qc,Ccl5,C1qb,C1qa,Jun
mmu04621	NOD-like receptor signaling pathway	6	164	0.72	0.0294	Ccl5,Oas1a,Gbp3,Jun,Ifi204,Irf9
mmu05164	Influenza A	6	165	0.72	0.0294	Ifih1,Ccl5,Ddx58,Oas1a,Jun,Irf9

Table 4. Enriched KEGG Pathways in arsenic-exposed GD18 Heart Tissue. Enriched KEGG pathways were also identified by STRING based on the 150 differentially expressed (comparing exposed to controls exhibited an unadjusted *p*-value <0.01) genes from the heart. The specific term identification number is reported along with its term description. Each protein from the differentially expressed input that are associated with that pathway are listed in the right column of the table. Data shown represents an N=3.

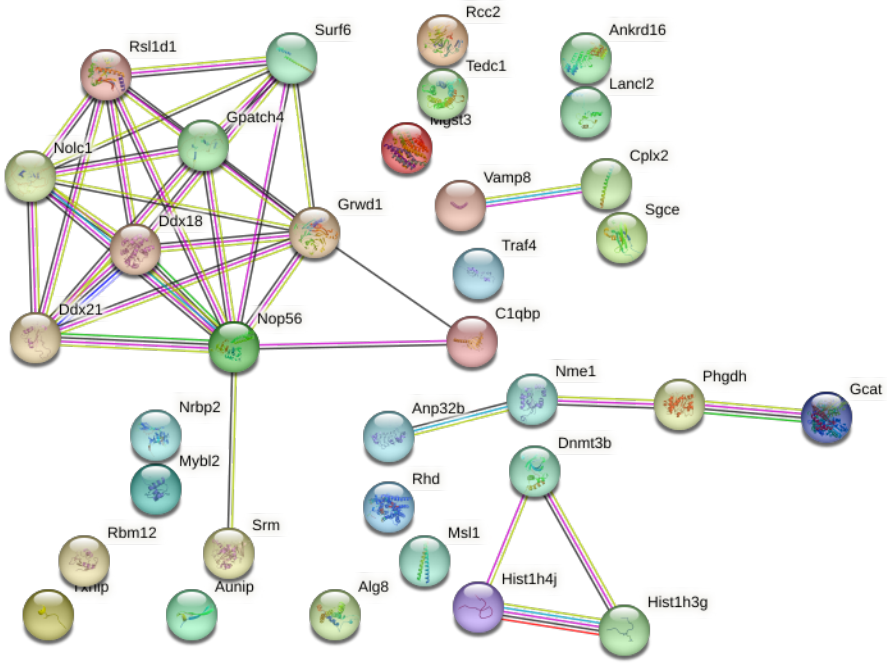

Figure 6. Lung STRING Map. Lung samples were obtained from gestational day (GD) 18 C57Bl/6J fetal mice exposed for 2 weeks prior to conception and during gestation to either 0 ppb (control) or 100 ppb (exposed) sodium (meta) arsenite. After microarray analysis, 41 differentially expressed (comparing exposed to controls exhibited an unadjusted *p*-value <0.01) genes from the lung were entered into the STRING database to generate a map. Nodes are indicated by colored circles; lines denote connections between nodes. Data shown represents an N=3.

A.

#term ID	term description	observed gene count	background gene count	strength	false discovery rate	matching proteins in your network (IDs)	matching proteins in your network (labels)
GO:0031497	Chromatin assembly	5	115	1.45	0.0138	10090.ENSMUSP00000079670,10090.ENSMUSP00000085006,10090.ENSMUSP00000099990,10090.ENSMUSP00000105396,10090.ENSMUSP00000116252	Hist1h3g,Hist1h4j,Anp32b,Dnmt3b,Grwd1
GO:0042254	Ribosome biogenesis	6	278	1.15	0.0138	10090.ENSMUSP00000001724,10090.ENSMUSP00000042691,10090.ENSMUSP00000048457,10090.ENSMUSP00000077612,10090.ENSMUSP00000099487,10090.ENSMUSP00000113431	Ddx18,Ddx21,Surf6,C1qbp,Nop56,Rsl1d1
GO:0044085	Cellular component biogenesis	14	2201	0.62	0.0138	10090.ENSMUSP00000001724,10090.ENSMUSP00000018005,10090.ENSMUSP00000042691,10090.ENSMUSP00000048457,10090.ENSMUSP00000059501,10090.ENSMUSP00000071163,10090.ENSMUSP00000077612,10090.ENSMUSP00000079670,10090.ENSMUSP00000085006,10090.ENSMUSP00000099487,10090.ENSMUSP00000099990,10090.ENSMUSP00000105396,10090.ENSMUSP00000113431,10090.ENSMUSP00000116252	Ddx18,Mybl2,Ddx21,Surf6,Vamp8,Rcc2,C1qbp,Hist1h3g,Hist1h4j,Nop56,Anp32b,Dnmt3b,Rsl1d1,Grwd1
GO:0006334	Nucleosome assembly	4	78	1.52	0.0162	10090.ENSMUSP00000079670,10090.ENSMUSP00000085006,10090.ENSMUSP00000099990,10090.ENSMUSP00000116252	Hist1h3g,Hist1h4j,Anp32b,Grwd1

B.

#term ID	term description	observed gene count	background gene count	strength	false discovery rate	matching proteins in your network (IDs)	matching proteins in your network (labels)
mmu00270	Cysteine and methionine metabolism	3	50	1.59	0.0246	10090.ENSMUSP00000006611,10090.ENSMUSP00000064755,10090.ENSMUSP00000105396	Srm,Phgdh,Dnmt3b

Table 5. Enriched Biological Processes (A) and Enriched KEGG Pathways (B) in arsenic-exposed GD18 Lung Tissue. Along with generation of the STRING map, **(A)** enriched biological processes and **(B)** KEGG pathways were identified based on the 41 differentially expressed (comparing exposed to controls exhibited an unadjusted *p*-value <0.01) genes from the lung using gene ontology (GO) and KEGG terms. The specific GO number or KEGG term ID number is reported along with its term description. Each protein from the differentially expressed input that are associated with that biological process or pathway are listed in the right column of the tables. Data shown represents an N=3.

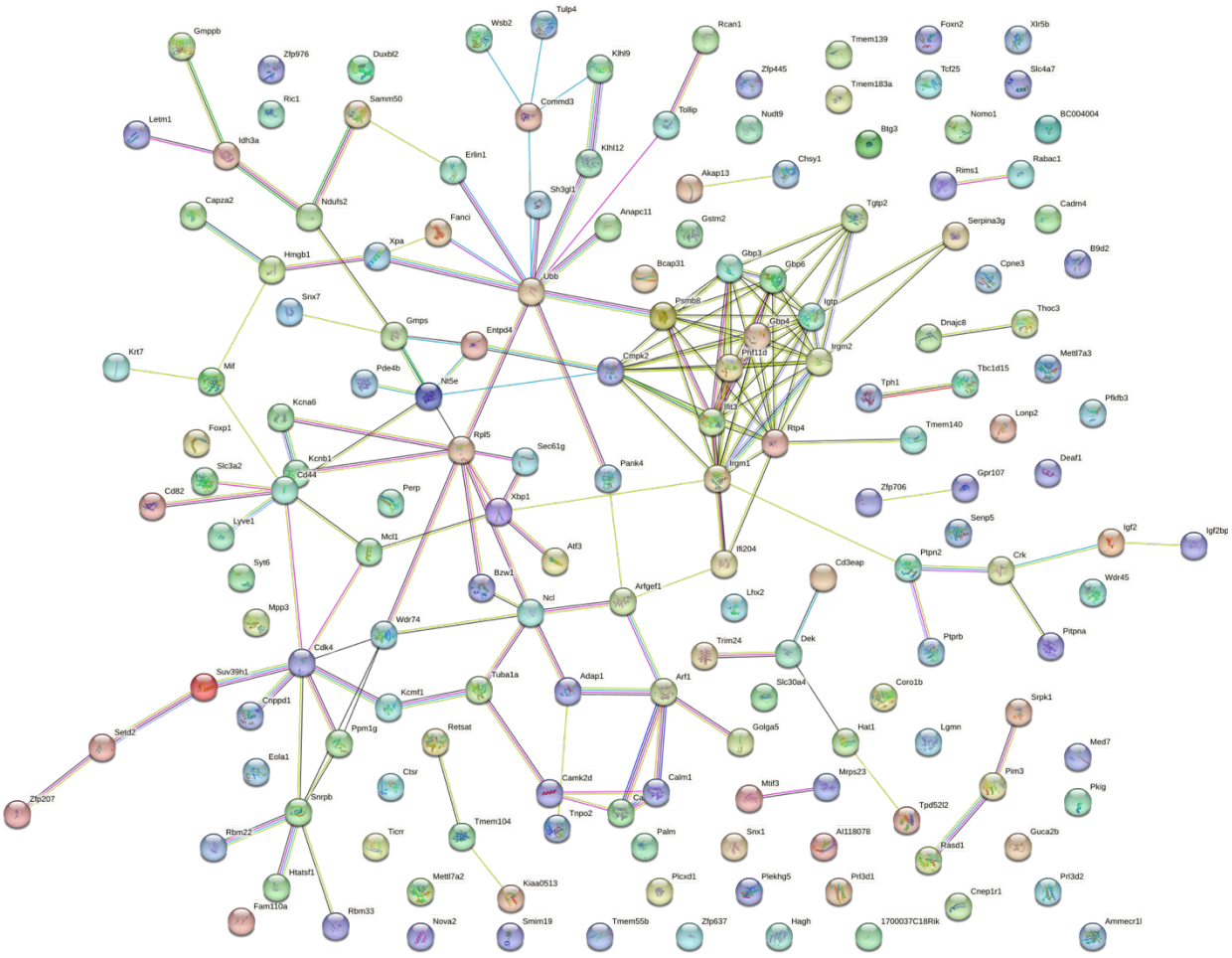

Figure 7. Placenta STRING Map. Placenta samples were obtained from gestational day (GD) 18 C57Bl/6J fetal mice exposed for 2 weeks prior to conception and during gestation to either 0 ppb (control) or 100 ppb (exposed) sodium (meta) arsenite. After microarray analysis, 165 differentially expressed (comparing exposed to controls exhibited an unadjusted *p*-value <0.01) genes from the placenta were entered into the STRING database to generate a map. Nodes are indicated by colored circles; lines denote connections between nodes. Data shown represents an N=3.

#term ID	term description	observed gene count	background gene count	strength	false discovery rate	matching proteins in your network (labels)
GO:0005622	Intracellular	125	12596	0.13	0.00014	Lhx2,Tollip,Bcap31,Sh3gl1,Cd44,Letm1,Slc30a4,Cdk4,Coro1b,Gstm2,Ndufs2,Capza2,Crk,Calm3,Ubb,Perp,Tbc1d15,Cmpk2,Lgmn,Dek,Ctsr,Samm50,Senp5,Btg3,Mrps23,Psmb8,Rbm22,Thoc3,Ncl,Atf3,Gmps,Snx7,Cpne3,Xpa,Pank4,Ppm1g,Nudt9,Trim24,Lonp2,AI118078,Snx1,Nt5e,Tph1,Palm,Rtp4,Mif,Serpina3g,Ticrr,Wdr74,Ric1,Mcl1,Pim3,Cd3eap,Fanci,Chsy1,Tulp4,Commd3,Irgm1,Bzw1,Rasd1,Zfp207,Xbp1,Zfp445,Tcf25,Gpr107,Kcnb1,Slc4a7,Rcan1,Mtif3,Kcmf1,BC004004,Retsat,Krt7,Rabac1,Zfp706,Deaf1,Arf1,Rpl5,Plekhg5,Hmgb1,Plcxd1,Arfgef1,Htatsf1,Syt6,Dnajc8,Klhl9,Cnep1r1,Tuba1a,Rims1,Igf2bp2,Anapc11,Snrpb,Ifit3,Gbp3,Camk2d,B9d2,Med7,Pkig,Fam110a,Calm1,Ifi204,Hat1,Klhl12,Gmppb,Suv39h1,Wdr45,Ptpn2,Hagh,Pitpna,Srpk1,Setd2,Akap13,Tpd52l2,Zfp637,Phf11d,Tmem55b,Idh3a,Erlin1,Slc3a2,Sec61g,Cnppd1,Tnpo2,Foxp1,Golga5,Entpd4
GO:0005737	Cytoplasm	106	10283	0.15	0.00077	Tollip,Bcap31,Sh3gl1,Cd44,Letm1,Slc30a4,Cdk4,Coro1b,Gstm2,Ndufs2,Capza2,Crk,Calm3,Ubb,Perp,Tbc1d15,Cmpk2,Lgmn,Dek,Ctsr,Samm50,Btg3,Mrps23,Psmb8,Rbm22,Ncl,Gmps,Snx7,Cpne3,Xpa,Pank4,Nudt9,Trim24,Lonp2,AI118078,Snx1,Nt5e,Tph1,Palm,Rtp4,Mif,Serpina3g,Ric1,Mcl1,Pim3,Cd3eap,Fanci,Chsy1,Tulp4,Commd3,Irgm1,Bzw1,Rasd1,Zfp207,Xbp1,Gpr107,Kcnb1,Slc4a7,Rcan1,Mtif3,Kcmf1,BC004004,Krt7,Rabac1,Zfp706,Deaf1,Arf1,Rpl5,Plekhg5,Hmgb1,Plcxd1,Arfgef1,Syt6,Dnajc8,Cnep1r1,Tuba1a,Rims1,Igf2bp2,Anapc11,Snrpb,Ifit3,Gbp3,Camk2d,B9d2,Pkig,Fam110a,Calm1,Ifi204,Klhl12,Gmppb,Wdr45,Ptpn2,Hagh,Pitpna,Srpk1,Akap13,Tpd52l2,Tmem55b,Idh3a,Erlin1,Slc3a2,Sec61g,Tnpo2,Foxp1,Golga5,Entpd4
GO:0043227	Membrane-bounded organelle	107	10370	0.15	0.00077	Lhx2,Tollip,Bcap31,Sh3gl1,Cd44,Letm1,Slc30a4,Cdk4,Ndufs2,Calm3,Ubb,Perp,Tbc1d15,Cmpk2,Lgmn,Dek,Ctsr,Samm50,Senp5,Btg3,Mrps23,Psmb8,Rbm22,Thoc3,Ncl,Atf3,Snx7,Cpne3,Xpa,Pank4,Ppm1g,Nudt9,Trim24,Nomo1,Lonp2,Snx1,Nt5e,Palm,Mif,Serpina3g,Ticrr,Wdr74,Ric1,Mcl1,Cd3eap,Fanci,Chsy1,Commd3,Irgm1,Rasd1,Zfp207,Xbp1,Zfp445,Tcf25,Gpr107,Kcnb1,Slc4a7,Rcan1,Mtif3,BC004004,Retsat,Rabac1,Zfp706,Deaf1,Arf1,Rpl5,Plekhg5,Hmgb1,Arfgef1,Htatsf1,Syt6,Dnajc8,Cnep1r1,Tuba1a,Rims1,Igf2bp2,Anapc11,Snrpb,Ifit3,Gbp3,Camk2d,B9d2,Med7,Pkig,Calm1,Ifi204,Hat1,Klhl12,Gmppb,Suv39h1,Ptpn2,Hagh,Srpk1,Setd2,Akap13,Zfp637,Phf11d,Tmem55b,Idh3a,Erlin1,Slc3a2,Sec61g,Cnppd1,Tnpo2,Foxp1,Golga5,Entpd4
GO:0043229	Intracellular organelle	111	11084	0.13	0.00077	Lhx2,Tollip,Bcap31,Sh3gl1,Cd44,Letm1,Slc30a4,Cdk4,Coro1b,Ndufs2,Capza2,Crk,Calm3,Ubb,Perp,Tbc1d15,Cmpk2,Lgmn,Dek,Ctsr,Samm50,Senp5,Btg3,Mrps23,Psmb8,Rbm22,Thoc3,Ncl,Atf3,Snx7,Cpne3,Xpa,Pank4,Ppm1g,Nudt9,Trim24,Lonp2,Snx1,Nt5e,Palm,Mif,Serpina3g,Ticrr,Wdr74,Ric1,Mcl1,Cd3eap,Fanci,Chsy1,Commd3,Irgm1,Rasd1,Zfp207,Xbp1,Zfp445,Tcf25,Gpr107,Kcnb1,Slc4a7,Rcan1,Mtif3,BC004004,Retsat,Krt7,Rabac1,Zfp706,Deaf1,Arf1,Rpl5,Plekhg5,Hmgb1,Arfgef1,Htatsf1,Syt6,Dnajc8,Cnep1r1,Tuba1a,Rims1,Igf2bp2,Anapc11,Snrpb,Ifit3,Gbp3,Camk2d,B9d2,Med7,Pkig,Fam110a,Calm1,Ifi204,Hat1,Klhl12,Gmppb,Suv39h1,Ptpn2,Hagh,Srpk1,Setd2,Akap13,Zfp637,Phf11d,Tmem55b,Idh3a,Erlin1,Slc3a2,Sec61g,Cnppd1,Tnpo2,Foxp1,Golga5,Entpd4
GO:0043231	Intracellular membrane-bounded organelle	100	9507	0.16	0.00077	Lhx2,Tollip,Bcap31,Cd44,Letm1,Slc30a4,Cdk4,Ndufs2,Calm3,Ubb,Perp,Tbc1d15,Cmpk2,Lgmn,Dek,Ctsr,Samm50,Senp5,Btg3,Mrps23,Psmb8,Rbm22,Thoc3,Ncl,Atf3,Cpne3,Xpa,Pank4,Ppm1g,Nudt9,Trim24,Lonp2,Snx1,Nt5e,Palm,Mif,Serpina3g,Ticrr,Wdr74,Ric1,Mcl1,Cd3eap,Fanci,Chsy1,Commd3,Irgm1,Rasd1,Zfp207,Xbp1,Zfp445,Tcf25,Gpr107,Kcnb1,Rcan1,Mtif3,BC004004,Retsat,Rabac1,Zfp706,Deaf1,Arf1,Rpl5,Hmgb1,Arfgef1,Htatsf1,Syt6,Dnajc8,Cnep1r1,Igf2bp2,Anapc11,Snrpb,Ifit3,Gbp3,Camk2d,B9d2,Med7,Pkig,Calm1,Ifi204,Hat1,Klhl12,Gmppb,Suv39h1,Ptpn2,Hagh,Srpk1,Setd2,Akap13,Zfp637,Phf11d,Tmem55b,Idh3a,Erlin1,Slc3a2,Sec61g,Cnppd1,Tnpo2,Foxp1,Golga5,Entpd4
GO:0043226	Organelle	113	11550	0.12	0.00151	Lhx2,Tollip,Bcap31,Sh3gl1,Cd44,Letm1,Slc30a4,Cdk4,Coro1b,Ndufs2,Capza2,Crk,Calm3,Ubb,Perp,Tbc1d15,Cmpk2,Lgmn,Dek,Ctsr,Samm50,Senp5,Btg3,Mrps23,Psmb8,Rbm22,Thoc3,Ncl,Atf3,Snx7,Cpne3,Xpa,Pank4,Ppm1g,Nudt9,Trim24,Nomo1,Lonp2,Snx1,Nt5e,Palm,Mif,Serpina3g,Ticrr,Guca2b,Wdr74,Ric1,Mcl1,Cd3eap,Fanci,Chsy1,Commd3,Irgm1,Rasd1,Zfp207,Xbp1,Zfp445,Tcf25,Gpr107,Kcnb1,Slc4a7,Rcan1,Mtif3,BC004004,Retsat,Krt7,Rabac1,Zfp706,Deaf1,Arf1,Rpl5,Plekhg5,Hmgb1,Arfgef1,Htatsf1,Syt6,Dnajc8,Cnep1r1,Tuba1a,Rims1,Igf2bp2,Anapc11,Snrpb,Ifit3,Gbp3,Camk2d,B9d2,Med7,Pkig,Fam110a,Calm1,Ifi204,Hat1,Klhl12,Gmppb,Suv39h1,Ptpn2,Hagh,Srpk1,Setd2,Akap13,Zfp637,Phf11d,Tmem55b,Idh3a,Erlin1,Slc3a2,Sec61g,Cnppd1,Tnpo2,Foxp1,Golga5,Entpd4
GO:0005634	Nucleus	72	6330	0.19	0.0039	Lhx2,Tollip,Cd44,Cdk4,Ndufs2,Calm3,Ubb,Dek,Senp5,Btg3,Mrps23,Psmb8,Rbm22,Thoc3,Ncl,Atf3,Cpne3,Xpa,Pank4,Ppm1g,Nudt9,Trim24,Lonp2,Nt5e,Palm,Mif,Serpina3g,Ticrr,Wdr74,Mcl1,Cd3eap,Fanci,Commd3,Rasd1,Zfp207,Xbp1,Zfp445,Tcf25,Gpr107,Rcan1,BC004004,Retsat,Zfp706,Deaf1,Rpl5,Hmgb1,Arfgef1,Htatsf1,Dnajc8,Cnep1r1,Igf2bp2,Anapc11,Snrpb,Gbp3,Camk2d,B9d2,Med7,Pkig,Calm1,Ifi204,Hat1,Suv39h1,Ptpn2,Srpk1,Setd2,Akap13,Zfp637,Phf11d,Slc3a2,Cnppd1,Tnpo2,Foxp1
GO:0110165	Cellular anatomical entity	138	15632	0.08	0.0039	Lhx2,Tollip,Bcap31,Sh3gl1,Cd44,Letm1,Slc30a4,Cdk4,Coro1b,Gstm2,Ndufs2,Capza2,Crk,Calm3,Ubb,Perp,Tbc1d15,Cmpk2,Lgmn,Dek,Ctsr,Samm50,Senp5,Btg3,Mrps23,Psmb8,Rbm22,Thoc3,Ncl,Atf3,Cd82,Gmps,Snx7,Cpne3,Xpa,Pank4,Ppm1g,Nudt9,Trim24,Lyve1,Nomo1,Lonp2,AI118078,Snx1,Nt5e,Tph1,Palm,Rtp4,Mif,Serpina3g,Ticrr,Guca2b,Wdr74,Ric1,Mcl1,Pim3,Cd3eap,Fanci,Tmem183a,Chsy1,Tulp4,Commd3,Irgm1,Bzw1,Rasd1,Zfp207,Xbp1,Zfp445,Tcf25,Gpr107,Tmem104,Kcnb1,Slc4a7,Rcan1,Mtif3,Kcmf1,BC004004,Cadm4,Retsat,Krt7,Tmem140,Rabac1,Zfp706,Deaf1,Arf1,Prl3d1,Rpl5,Plekhg5,Hmgb1,Plcxd1,Arfgef1,Htatsf1,Syt6,Ptprb,Dnajc8,Klhl9,Cnep1r1,Tuba1a,Rims1,Igf2bp2,Anapc11,Snrpb,Ifit3,Igf2,Gbp3,Camk2d,B9d2,Med7,Pkig,Fam110a,Calm1,Ifi204,Hat1,Klhl12,Kcna6,Gmppb,Suv39h1,Wdr45,Ptpn2,Hagh,Pitpna,Srpk1,Setd2,Akap13,Tpd52l2,Zfp637,Phf11d,Tmem55b,Idh3a,Erlin1,Slc3a2,Smim19,Sec61g,Cnppd1,Tnpo2,Foxp1,Golga5,Entpd4
GO:0005654	Nucleoplasm	43	3261	0.25	0.0148	Lhx2,Tollip,Cdk4,Ndufs2,Calm3,Ubb,Dek,Psmb8,Rbm22,Thoc3,Ncl,Atf3,Cpne3,Xpa,Ppm1g,Nudt9,Trim24,Nt5e,Palm,Mif,Ticrr,Wdr74,Mcl1,Cd3eap,Fanci,Zfp207,Gpr107,Deaf1,Rpl5,Arfgef1,Htatsf1,Dnajc8,Anapc11,Snrpb,Med7,Calm1,Ifi204,Hat1,Suv39h1,Ptpn2,Srpk1,Phf11d,Slc3a2
GO:0031981	Nuclear lumen	46	3771	0.22	0.0439	Lhx2,Tollip,Cdk4,Ndufs2,Calm3,Ubb,Dek,Senp5,Psmb8,Rbm22,Thoc3,Ncl,Atf3,Cpne3,Xpa,Ppm1g,Nudt9,Trim24,Nt5e,Palm,Mif,Ticrr,Wdr74,Mcl1,Cd3eap,Fanci,Zfp207,Gpr107,BC004004,Deaf1,Rpl5,Hmgb1,Arfgef1,Htatsf1,Dnajc8,Anapc11,Snrpb,Med7,Calm1,Ifi204,Hat1,Suv39h1,Ptpn2,Srpk1,Phf11d,Slc3a2

Table 6. Top 10 Enriched cellular components in arsenic-exposed GD18 Placenta Tissue. Along with generation of the STRING map, enriched cellular components were identified based on the 165 differentially expressed (comparing exposed to controls exhibited an unadjusted *p*-value <0.01) genes from the placenta using gene ontology (GO). The specific GO number is reported along with its term

description. Each protein from the differentially expressed input that are associated with that biological process are listed in the right column of the table. Data shown represents an N=3.

Supplemental Data

Table S1. Complete List of Differential Gene Expression Analysis for Heart Tissue. Heart samples were obtained from gestational day (GD) 18 C57Bl/6J fetal mice exposed for 2 weeks prior to conception and during gestation to either 0 ppb (control) or 100 ppb (exposed) sodium (meta) arsenite. After microarray analysis, the expression of all genes from heart tissue were compared for arsenic exposed to unexposed controls. Data shown represents an N=3.

Table S2. Complete List of Differential Gene Expression Analysis for Liver Tissue. Liver samples were obtained from gestational day (GD) 18 C57Bl/6J fetal mice exposed for 2 weeks prior to conception and during gestation to either 0 ppb (control) or 100 ppb (exposed) sodium (meta) arsenite. After microarray analysis, the expression of all genes from liver tissue were compared for arsenic exposed to unexposed controls. Data shown represents an N=3.

Table S3. Complete List of Differential Gene Expression Analysis for Lung Tissue. Lung samples were obtained from gestational day (GD) 18 C57Bl/6J fetal mice exposed for 2 weeks prior to conception and during gestation to either 0 ppb (control) or 100 ppb (exposed) sodium (meta) arsenite. After microarray analysis, the expression of all genes from lung tissue were compared for arsenic exposed to unexposed controls. Data shown represents an N=3.

Table S4. Complete List of Differential Gene Expression Analysis for Placenta Tissue. Placenta samples were obtained from gestational day (GD) 18 C57Bl/6J fetal mice exposed for 2 weeks prior to conception

and during gestation to either 0 ppb (control) or 100 ppb (exposed) sodium (meta) arsenite. After microarray analysis, the expression of all genes from placenta tissue were compared for arsenic exposed to unexposed controls. Data shown represents an N=3.

Table S5. Complete List of Enriched Biological Processes in arsenic-exposed GD18 Liver Tissue. Enriched biological processes were identified in STRING based on the 240 differentially expressed (comparing exposed to controls exhibited an unadjusted *p*-value <0.01) genes from the liver using gene ontology (GO). The specific GO number is reported along with its term description. Each protein from the differentially expressed input that are associated with that biological process are listed in the right column of the table. Data shown represents an N=3.

Reference List

1. Ayotte JD, Medalie L, Qi SL, Backer LC, Nolan BT. 2017. Estimating the High-Arsenic Domestic-Well Population in the Conterminous United States. Environ Sci Technol. 51(21):12443–12454. doi:10.1021/acs.est.7b02881.

2. Caldwell KE, Labrecque MT, Solomon BR, Ali A, Allan AM. 2015. Prenatal arsenic exposure alters the programming of the glucocorticoid signaling system during embryonic development. Neurotoxicology and Teratology. 47:66–79. doi:10.1016/j.ntt.2014.11.006.

3. Demanelis K, Argos M, Tong L, Shinkle J, Sabarinathan M, Rakibuz-Zaman M, Sarwar G, Shahriar H, Islam T, Rahman M, et al. 2019. Association of Arsenic Exposure with Whole Blood DNA Methylation: An Epigenome-Wide Study of Bangladeshi Adults. Environmental Health Perspectives. 127(5):057011. doi:10.1289/EHP3849.

4. Espíndola S, Vilches-Flores A, Hernández-Echeagaray E. 2012. 3-Nitropropionic acid modifies neurotrophin mRNA expression in the mouse striatum: 18S-rRNA is a reliable control gene for studies of the striatum. Neurosci Bull. 28(5):517–531. doi:10.1007/s12264-012-1259-x.

5. Everitt AR, Clare S, Pertel T, John SP, Wash RS, Smith SE, Chin CR, Feeley EM, Sims JS, Adams DJ, et al. 2012. IFITM3 restricts the morbidity and mortality associated with influenza. Nature. 484(7395):519–523. doi:10.1038/nature10921.

6. Farzan SF, Li Z, Korrick SA, Spiegelman D, Enelow R, Nadeau K, Baker E, Karagas MR. 2016. Infant Infections and Respiratory Symptoms in Relation to in Utero Arsenic Exposure in a U.S. Cohort. Environ Health Perspect. 124(6):840–847. doi:10.1289/ehp.1409282.

7. Fry RC, Navasumrit P, Valiathan C, Svensson JP, Hogan BJ, Luo M, Bhattacharya S, Kandjanapa K, Soontararuks S, Nookabkaew S, et al. 2007. Activation of Inflammation/NF-κB Signaling in Infants Born to Arsenic-Exposed Mothers. PLOS Genetics. 3(11):e207. doi:10.1371/journal.pgen.0030207.

8. García Salcedo JJ, Roh T, Nava Rivera LE, Betancourt Martínez ND, Carranza Rosales P, San Miguel Salazar MF, Rivera Guillén MA, Serrano Gallardo LB, Niño Castañeda MS, Guzmán Delgado NE, et al. 2022. Comparative Biomonitoring of Arsenic Exposure in Mothers and Their Neonates in Comarca Lagunera, Mexico. Int J Environ Res Public Health. 19(23):16232. doi:10.3390/ijerph192316232.

9. Gene Ontology Consortium. 2004. The Gene Ontology (GO) database and informatics resource. Nucleic Acids Research. 32(90001):258D – 261. doi:10.1093/nar/gkh036.

10. Gómez-Herranz M, Nekulova M, Faktor J, Hernychova L, Kote S, Sinclair EH, Nenutil R, Vojtesek B, Ball KL, Hupp TR. 2019. The effects of IFITM1 and IFITM3 gene deletion on IFNγ stimulated protein synthesis. Cellular Signalling. 60:39–56. doi:10.1016/j.cellsig.2019.03.024.

11. He W, Greenwell RJ, Brooks DM, Calderón-Garcidueñas L, Beall HD, Coffin JD. 2007. Arsenic Exposure in Pregnant Mice Disrupts Placental Vasculogenesis and Causes Spontaneous Abortion. Toxicological Sciences. 99(1):244–253. doi:10.1093/toxsci/kfm162.

12. Hernández A, Sampayo-Reyes A, Marcos R. 2011. Identification of differentially expressed genes in the livers of chronically i-As-treated hamsters. Mutation Research/Fundamental and Molecular Mechanisms of Mutagenesis. 713(1):48–55. doi:10.1016/j.mrfmmm.2011.05.013.

13. Jiang L-Q, Xia T, Hu Y-H, Sun M-S, Yan S, Lei C-Q, Shu H-B, Guo J-H, Liu Y. 2018. IFITM3 inhibits virus-triggered induction of type I interferon by mediating autophagosome-dependent degradation of IRF3. Cell Mol Immunol. 15(9):858–867. doi:10.1038/cmi.2017.15.

14. Kadmiel M, Cidlowski JA. 2013. Glucocorticoid receptor signaling in health and disease. Trends Pharmacol Sci. 34(9):518–530. doi:10.1016/j.tips.2013.07.003.

15. Kanehisa M, Goto S. KEGG: kyoto encyclopedia of genes and genomes. Nucleic Acids Res. 2000 Jan 1;28(1):27-30. doi: 10.1093/nar/28.1.27. PMID: 10592173; PMCID: PMC102409.

16. Khan MdA, Hira-Smith M, Ahmed SI, Yunus M, Hasan SMT, Liaw J, Balmes J, Raqib R, Yuan Y, Kalman D, et al. 2020. Prospective cohort study of respiratory effects at ages 14 to 26 following early life exposure to arsenic in drinking water. Environ Epidemiol. 4(2):e089. doi:10.1097/EE9.0000000000000089.

17. Kitamura A, Maekawa Y, Uehara H, Izumi K, Kawachi I, Nishizawa M, Toyoshima Y, Takahashi H, Standley DM, Tanaka K, et al. 2011. A mutation in the immunoproteasome subunit PSMB8 causes autoinflammation and lipodystrophy in humans. J Clin Invest. 121(10):4150–4160. doi:10.1172/JCI58414.

18. Kozul CD, Ely KH, Enelow RI, Hamilton JW. Low-dose arsenic compromises the immune response to influenza A infection in vivo. Environ Health Perspect. 2009;117(9):1441-7. Epub 2009/09/15. doi: 10.1289/ehp.0900911. PubMed PMID: 19750111 PMCID: PMC2737023.

19. Laine JE, Fry RC. 2016. A Systems Toxicology-based Approach Reveals Biological Pathways Dysregulated by Prenatal Arsenic Exposure. 82(1):189. doi:10.1016/j.aogh.2016.01.015.

20. Li K, Markosyan RM, Zheng Y-M, Golfetto O, Bungart B, Li M, Ding S, He Y, Liang C, Lee JC, et al. 2013. IFITM proteins restrict viral membrane hemifusion. PLoS Pathog. 9(1):e1003124. doi:10.1371/journal.ppat.1003124.

21. Liu J, Xie Y, Cooper R, Ducharme DMK, Tennant R, Diwan BA, Waalkes MP. 2007. Transplacental exposure to inorganic arsenic at a hepatocarcinogenic dose induces fetal gene expression changes in mice indicative of aberrant estrogen signaling and disrupted steroid metabolism. Toxicol Appl Pharmacol. 220(3):284–291. doi:10.1016/j.taap.2007.01.018.

22. Lou K, Huang P, Ma H, Wang X, Xu H, Wang W. 2022. Orlistat increases arsenite tolerance in THP-1 derived macrophages through the up-regulation of ABCA1. Drug Chem Toxicol. 45(1):274–282. doi:10.1080/01480545.2019.1683571.

23. Meakin CJ, Martin EM, Szilagyi JT, Nylander-French LA, Fry RC. 2019. Inorganic Arsenic as an Endocrine Disruptor: Modulation of the Glucocorticoid Receptor Pathway in Placental Cells via CpG Methylation. Chem Res Toxicol. 32(3):493–499. doi:10.1021/acs.chemrestox.8b00352.

24. Myllynen P, Pasanen M, Pelkonen O. 2005. Human placenta: a human organ for developmental toxicology research and biomonitoring. Placenta. 26(5):361–371. doi:10.1016/j.placenta.2004.09.006.

25. Narayana SK, Helbig KJ, McCartney EM, Eyre NS, Bull RA, Eltahla A, Lloyd AR, Beard MR. 2015. The Interferon-induced Transmembrane Proteins, IFITM1, IFITM2, and IFITM3 Inhibit Hepatitis C Virus Entry. J Biol Chem. 290(43):25946–25959. doi:10.1074/jbc.M115.657346.

26. Naujokas MF, Anderson B, Ahsan H, Aposhian HV, Graziano JH, Thompson C, Suk WA. 2013. The broad scope of health effects from chronic arsenic exposure: update on a worldwide public health problem. EHP. 121(3):295–302. doi:10.1289/ehp.1205875.

27. Neerhof MG, Thaete LG. 2008. The Fetal Response to Chronic Placental Insufficiency. Seminars in Perinatology. 32(3):201–205. doi:10.1053/j.semperi.2007.11.002.

28. Nordmann A, Wixler L, Boergeling Y, Wixler V, Ludwig S. 2012. A new splice variant of the human guanylate-binding protein 3 mediates anti-influenza activity through inhibition of viral transcription and replication. FASEB J. 26(3):1290–1300. doi:10.1096/fj.11-189886.

29. Percie du Sert N, Ahluwalia A, Alam S, Avey MT, Baker M, Browne WJ, Clark A, Cuthill IC, Dirnagl U, Emerson M, Garner P, Holgate ST, Howells DW, Hurst V, Karp NA, Lazic SE, Lidster K, MacCallum CJ, Macleod M, Pearl EJ, Petersen OH, Rawle F, Reynolds P, Rooney K, Sena ES, Silberberg SD, Steckler T, Würbel H. Reporting animal research: Explanation and elaboration for the ARRIVE guidelines 2.0. PloS Biol. 2020 Jul 14;18(7):e3000411. Doi: 10.1371/journal.pbio.3000411. PMID: 32663221; PMCID: PMC7360025.

30. PubChem. PSMB8 - proteasome 20S subunit beta 8 (human). [accessed 2024 Apr 24]. https://pubchem.ncbi.nlm.nih.gov/gene/PSMB8/human.

31. Rager JE, Bailey KA, Smeester L, Miller SK, Parker JS, Laine JE, Drobná Z, Currier J, Douillet C, Olshan AF, et al. 2014. Prenatal arsenic exposure and the epigenome: altered microRNAs associated with

innate and adaptive immune signaling in newborn cord blood. Environ Mol Mutagen. 55(3):196–208. doi:10.1002/em.21842.

32. Ramsey KA, Bosco A, McKenna KL, Carter KW, Elliot JG, Berry LJ, Sly PD, Larcombe AN, Zosky GR. In utero exposure to arsenic alters lung development and genes related to immune and mucociliary function in mice. Environ Health Perspect. 2013;121(2):244-50. Epub 2012/12/12. doi: 10.1289/ehp.1205590. PubMed PMID: 23221970 PMCID: PMC3569690.
33. Ramsey KA, Foong RE, Sly PD, Larcombe AN, Zosky GR. Early life arsenic exposure and acute and long-term responses to influenza A infection in mice. Environ Health Perspect. 2013;121(10):1187-93. doi: 10.1289/ehp.1306748. PubMed PMID: 23968752 PMCID: PMCPMC3801203.
34. Renu K, Madhyastha H, Madhyastha R, Maruyama M, Arunachlam S, V.g. A. 2018. Role of arsenic exposure in adipose tissue dysfunction and its possible implication in diabetes pathophysiology. Toxicology Letters. 284:86–95. doi:10.1016/j.toxlet.2017.11.032.
35. Riffo-Campos AL, Fuentes-Trillo A, Tang WY, Soriano Z, De Marco G, Rentero-Garrido P, Adam-Felici V, Lendinez-Tortajada V, Francesconi K, Goessler W, et al. 2018. In silico epigenetics of metal exposure and subclinical atherosclerosis in middle aged men: pilot results from the Aragon Workers Health Study. Philos Trans R Soc Lond B Biol Sci. 373(1748):20170084. doi:10.1098/rstb.2017.0084.
36. Shannon P, Markiel A, Ozier O, Baliga NS, Wang JT, Ramage D, Amin N, Schwikowski B, Ideker T. 2003. Cytoscape: A Software Environment for Integrated Models of Biomolecular Interaction Networks. Genome Res. 13(11):2498–2504. doi:10.1101/gr.1239303.
37. Smith AH, Marshall G, Liaw J, Yuan Y, Ferreccio C, Steinmaus C. 2012. Mortality in Young Adults following in Utero and Childhood Exposure to Arsenic in Drinking Water. EHP. 120(11):1527–1531. doi:10.1289/ehp.1104867.

38. Song Y, Zhou T, Zong Y, Gu B, Tan X, Yang L. 2019. Arsenic inhibited cholesterol efflux of THP-1 macrophages via ROS-mediated ABCA1 hypermethylation. Toxicology. 424:152225. doi:10.1016/j.tox.2019.05.012.

39. States JC, Singh AV, Knudsen TB, Rouchka EC, Ngalame NO, Arteel GE, Piao Y, Ko MSH. 2012. Prenatal Arsenic Exposure Alters Gene Expression in the Adult Liver to a Proinflammatory State Contributing to Accelerated Atherosclerosis. PLOS ONE. 7(6):e38713. doi:10.1371/journal.pone.0038713.

40. Szklarczyk D, Kirsch R, Koutrouli M, Nastou K, Mehryary F, Hachilif R, Gable AL, Fang T, Doncheva NT, Pyysalo S, et al. 2023. The STRING database in 2023: protein–protein association networks and functional enrichment analyses for any sequenced genome of interest. Nucleic Acids Research. 51(D1):D638–D646. doi:10.1093/nar/gkac1000.

41. Theodoris CV, Xiao L, Chopra A, Chaffin MD, Al Sayed ZR, Hill MC, Mantineo H, Brydon EM, Zeng Z, Liu XS, et al. 2023. Transfer learning enables predictions in network biology. Nature. 618(7965):616–624. doi:10.1038/s41586-023-06139-9.

42. Torres L, Juárez U, García L, Miranda-Ríos J, Frias S. Microarray analysis of microRNA expression in mouse fetus at 13.5 and 14.5 days post-coitum in ear and back skin tissues. Genom Data. 2016 Jun 24;9:70-7. doi: 10.1016/j.gdata.2016.06.011. PMID: 27408816; PMCID: PMC4932619.

43. Vilmundarson RO, Heydarikhorneh N, Duong A, Ho T, Keyhanian K, Soheili F, Chen HH, Stewart AFR. Savior Siblings Might Rescue Fetal Lethality But Not Adult Lymphoma in Irf2bp2-Null Mice. Front Immunol. 2022 Jul 4;13:868053. doi: 10.3389/fimmu.2022.868053. PMID: 35865523; PMCID: PMC9295810.

44. Winterbottom EF, Ban Y, Sun X, Capobianco AJ, Marsit CJ, Chen X, Wang L, Karagas MR, Robbins DJ. 2019. Transcriptome-wide analysis of changes in the fetal placenta associated with prenatal arsenic

exposure in the New Hampshire Birth Cohort Study. Environmental Health. 18(1):100. doi:10.1186/s12940-019-0535-x.

45. Winterbottom EF, Moroishi Y, Halchenko Y, Armstrong DA, Beach PJ, Nguyen QP, Capobianco AJ, Ayad NG, Marsit CJ, Li Z, et al. 2019. Prenatal arsenic exposure alters the placental expression of multiple epigenetic regulators in a sex-dependent manner. Environmental Health. 18(1):18. doi:10.1186/s12940-019-0455-9.

46. Xie Y, Liu J, Benbrahim-Tallaa L, Ward JM, Logsdon D, Diwan BA, Waalkes MP. 2007. Aberrant DNA methylation and gene expression in livers of newborn mice transplacentally exposed to a hepatocarcinogenic dose of inorganic arsenic. Toxicology. 236(1–2):7–15. doi:10.1016/j.tox.2007.03.021.

47. Xu F-X, Chen X, Zhang H, Fan Y-J, Song Y-P, Lv J-W, Xie Y-L, Huang Y, Chen D-Z, Wang H, et al. 2022. Association between gestational arsenic exposure and intrauterine growth restriction: the role of folate content. Environ Sci Pollut Res Int. 29(59):89652–89661. doi:10.1007/s11356-022-21961-w.

48. Yang X-W, Wang P, Liu J-Q, Zhang H, Xi W-D, Jia X-H, Wang K-K. 2014. Coordinated regulation of the immunoproteasome subunits by PML/RARα and PU.1 in acute promyelocytic leukemia. Oncogene. 33(21):2700–2708. doi:10.1038/onc.2013.224.